Table 3
Adjusted mean levels of free TFPI, PAI-1, and von Willebrand factor according to rank of intimal-medial thickness (IMT) of the carotid artery

	IMT-rank				*P* for trend
	*Q*1	*Q*2	*Q*3	*Q*4	
Free TFPI (ng/ml)					
Men					
Age adjusted	15.3 ± 0.7	15.9 ± 0.5	17.5 ± 0.5‡	18.4 ± 0.6‡	0.003
All adjusted	16.2 ± 0.7	15.9 ± 0.5	17.2 ± 0.6	17.9 ± 0.6	0.075
Women					
Age adjusted	14.3 ± 0.7	15.8 ± 0.5‡	15.6 ± 0.5	14.8 ± 0.6	0.410
All adjusted	14.9 ± 0.6	15.9 ± 0.5	15.2 ± 0.5	14.5 ± 0.6	0.250
PAI-1 (ng/ml)					
Men					
Age adjusted	21.9 ± 4.9	31.1 ± 3.5	35.1 ± 4.2	39.8 ± 4.3‡	<0.001
All adjusted	24.1 ± 5.3	30.8 ± 3.5	34.7 ± 4.3	38.3 ± 4.5	<0.001
Women					
Age adjusted	18.0 ± 2.9	19.1 ± 2.1	26.3 ± 2.2‡	28.4 ± 2.7‡	0.227
All adjusted	20.3 ± 2.6	20.8 ± 1.9	23.7 ± 2.0	26.9 ± 2.5	0.317
von Willebrand factor (%)					
Men					
Age adjusted	144.0 ± 8.3	142.1 ± 6.0	135.6 ± 7.2	143.0 ± 7.3	0.353
All adjusted	141.3 ± 8.9	142.1 ± 6.0	136.9 ± 7.3	144.4 ± 7.7	0.180
Women					
Age adjusted	133.7 ± 7.6	134.0 ± 5.5	130.8 ± 5.9	131.8 ± 7.1	0.042
All adjusted	133.5 ± 7.7	134.7 ± 5.7	129.9 ± 6.0	132.0 ± 7.4	0.049

Values are mean ± errors adjusted for age or adjusted for age, life style (current drinking and smoking), body mass index, present illness (diabetes, hypercholesterolemia), systolic blood pressure, and hypertensive drug use. (‡) $P < 0.05$ compared with Q1 subjects. TFPI; tissue factor pathway inhibitor, PAI-1; plasminogen activator inhibitor-1.

levels in men were not detected after adjustment for several possible confounding factors (all adjusted). The free TFPI levels in women demonstrated a mountain-shaped relationship with the degree of IMT in the multivariate analysis.

Age-adjusted PAI-1 levels in men increased with increasing IMT rank ($P < 0.001$) and the levels in the fourth quartile compared to the lowest IMT quartile remained statistically significant in the multivariate analysis. Age-adjusted PAI-1 levels in women also increased with increasing IMT rank and the levels in the third and fourth quartiles compared to the lowest quartile were statistically significant, although the *P* value for trend was 0.227. The statistically significant increases of PAI-1 levels in men was detected after all adjustments.

In contrast, the age-adjusted vWF levels in both sexes did not show significant changes among IMT quartiles, although the *P* values for trend in women after all adjustments were significant. These results indicate that measurement of the levels of free TFPI and PAI-1 is a potentially useful tool for the detection of early atherosclerosis in men.

4. Discussion

In this cross-sectional analysis, we have demonstrated that increased levels of free TFPI and PAI-1 in men without CVD were closely associated with the elevation of IMT in common carotid arteries as measured by B-mode ultrasonography. These findings suggest that free TFPI and PAI-1 may be sensitive markers reflecting early atherosclerosis in the carotid arteries.

It has been demonstrated that TFPI localizes with tissue factor within atherosclerotic plaques in human carotid and coronary arteries and modulates the thrombogenicity of the plaque by attenuating the tissue factor activity [18–20]. Enhancement of TFPI expression in the atherosclerotic plaque will cause an increase in the free TFPI concentration in the plasma of patients with cardiovascular disease. In fact, elevated free TFPI levels have been reported in the plasma of patients with ischemic heart disease [21,22]. These findings imply that an elevated level of free TFPI in the plasma is closely associated with hypercoagulable states in atherosclerotic diseases. However, the role of TFPI associated with subclinical or early atherosclerosis was rarely reported. Sakkinen et al. reported a significant positive relationship between the level of plasma TFPI activity and subclinical cardiovascular disease in a healthy elderly cohort study [23]. However, the relationship between age/gender and TFPI levels in a general population has not been examined in detail. In this study, we have extended the above results and demonstrated a direct link between the extent of carotid artery atherosclerosis and the plasma level of free TFPI antigen in men in a Japanese general population without CVD.

As summarized in review articles [24,25], many investigators have demonstrated the crucial role of PAI-1 in human atherothrombosis. High plasma PAI-1 concentrations are associated with various thrombotic diseases and are independent risk factors for myocardial infarction, as has been proven by epidemiological studies. Animal experiments using PAI-1 transgenic mice and PAI-1 knock-out mice also support the role of PAI-1 in the progression of atherosclerosis [26–28]. These previous findings suggest that an increased PAI-1 level in the plasma is closely associated with the progression of atherosclerotic conditions. Here, we have demonstrated that this relationship could also be observed in early atherosclerotic conditions in a general population.

We have previously reported that the mean IMT value of both sexes increased stepwise with the number of major coronary risk factors, namely hypertension, smoking, and hypercholesterolemia [5]. It has also been reported that PAI-1 levels were increased in patients with early hypertension, and that these elevated PAI-1 levels were improved by treatment with angiotensin-converting enzyme inhibitor [29]. Recently, it has been reported that PAI-1 deficiency prevents hypertension and vascular fibrosis in response to long-term nitric oxide synthase inhibition [30]. Taken together, these data indicate that early atherosclerotic conditions or endothelial cell dysfunction are induced by hypertensive conditions, resulting in elevation of the plasma levels of free TFPI and PAI-1. Therefore, it is thought that the close association between elevation of the plasma levels of free TFPI and PAI-1 and hypertensive conditions probably diminished the statistically independent association between plasma levels of free TFPI and PAI-1 and the degree of IMT.

In conclusion, we have demonstrated that the levels of free TFPI and PAI-1 in men increased with the degree of IMT. Therefore, we propose that free TFPI and PAI-1 are potentially useful markers for detecting early atherosclerosis. However, prospective studies are necessary to clarify whether these markers are predictive of the onset of atherosclerotic diseases in Japanese people.

Acknowledgements

This study was supported by Health Sciences Research Grants for Research on Specific Diseases, Blood Coagulation Disorders from the Ministry of Health, Labour and Welfare of Japan, the Program for Promotion of Fundamental Studies in Health Sciences of the Organization for Pharmaceutical Safety and Research (of Japan), Special Coordination Funds for Promoting Science and Technology, a Grant-in-Aid for Scientific Research from the Ministry of Education, Culture, Sports, Science and Technology of the Japanese Government and a Grant-in-Aid for Cancer Research and for the second term of a Comprehensive Ten-Year Strategy for Cancer Control from the Ministry of Health and Welfare of Japan. We would like to express our highest gratitude to the following people for their continuous support to our population survey in this area: Dr. Otosaburo Hishikawa, the president of the Suita medical association, Dr. Katsuyuki Kawanishi, a committee in chief for municipal health check-up services and other members of the Suita City Medical Association, and Mr. Shigeru Kobayashi, the director of the City Health Center. We also express our greatest thanks to the members of the attendants' society (Satsuki-Junyu-kai) for their cooperation and assistance to the study.

References

[1] Hodis HN, Mack WJ. Risk factor assessment, treatment strategy and prevention of coronary artery disease: the need for a more rational approach. J Intern Med 1994;236:111–3.
[2] Blankenhorn DH, Hodis HN. Arteial imaging and atherosclerosis reversal. Arterioscler Thromb 1994;14:177–92.
[3] Geroulakos G, O'Gorman DJ, Kalodiki E, Sheridan GJ, Nicolaides AN. The carotid intima-media thickness as a marker of the presence of severe symptomatic coronary artery disease. Eur Heart J 1994;15:781–5.
[4] Crouse III JR, Craven TE, Hagaman AP, Bond MG. Association of coronary disease with segment-specific intimal-medial thickening of the extracranial carotid artery. Circulation 1995;92:1141–7.
[5] Mannami T, Baba S, Ogata J. Strong and significant relationships between aggregation of major coronary risk factors and the acceleration of carotid atherosclerosis in the general population of a Japanese city: the Suita Study. Arch Intern Med 2000;160:2297–303.
[6] Hunt KJ, Pankow JS, Offenbacher S, et al. B-mode ultrasound-detected carotid artery lesions with and without acoustic shadowing and their association with markers of inflammation and endothelial activation: the atherosclerosis risk in communities study. Atherosclerosis 2002;162:145–55.
[7] Wu KK, Folsom AR, Heiss G, et al. Association of coagulation factors and inhibitors with carotid artery atherosclerosis; early results of the athrosclerosis risk in communities (ARIC) study. Ann Epidemiol 1992;2:471–80.
[8] Folsom AR, Wu KK, Shahar E, Davis CE. For the athrosclerosis risk in communities (ARIC) study investigators. Association of hemostatic variables with prevalent cardiovascular disease and asymptomatic carotid artery atherosclerosis. Arterioscler Thromb 1993;13:1829–36.
[9] Salomaa V, Stinson V, Kark JD, et al. Association of fibrinolytic parameters with early atherosclerosis. The ARIC study. Circulation 1995;91:284–90.
[10] Thompson SG, Kienast J, Pyke SD, Haverkate F, van de Loo JC. Hemostatic factors and the risk of myocardial infarction or sudden death in patients with angina pectoris. European Concerted Action on Thrombosis and Disabilities Angina Pectoris Study Group. N Engl J Med 1995;332:635–41.
[11] Kumari M, Marmot M, Brunner E. Social determinants of von Willebrand factor: the Whitehall II study. Arterioscler Thromb Vasc Biol 2000;20:1842–7.
[12] Bajaj MS, Birktoft JJ, Steer SA, Bajaj SP. Structure and biology of tissue factor pathway inhibitor. Thromb Haemost 2001;86:959–72.
[13] Kato H. Regulation of functions of vascular wall cells by tissue factor pathway inhibitor: basic and clinical aspects. Arterioscler Thromb Vasc Biol 2002;22:539–648.
[14] Morange PE, Renucci JF, Charles MA, et al. Plasma levels of free and total TFPI, relationship with cardiovascular risk factors and endothelial cell markers. Thromb Haemost 2001;85:999–1003.
[15] Kokawa T, Enjyoji K, Kumeda K, et al. Measurement of the free form of TFPI antigen in hyperlipidemia: relationship between free

and endothelial cell-associated forms of TFPI. Arterioscler Thromb Vasc Biol 1996;16:802–8.
[16] Mannami T, Konishi M, Baba S, Nishi N, Terao A. Prevalence of asymptomatic carotid atherosclerotic lesions detected by high-resolution ultrasonography and its relation to cardiovascular risk factors in the general population of a Japanese city: The Suita Study. Stroke 1997;28:518–25.
[17] Abumiya T, Enjyoji K, Kokawa T, Kamikubo Y, Kato H. An anti-tissue factor pathway inhibitor (TFPI) monoclonal antibody recognized the third Kunitz domain (K3) of free-form of TFPI but not liporotein-associated forms in plasma. J Biochem 1995;118:178–82.
[18] Caplice NM, Mueske CS, Kleppe LS, Simari RD. Presence of tissue factor pathway inhibitor in human atherosclerotic plaques is associated with reduced tissue factor activity. Circulation 1998;98:1051–7.
[19] Kaikita K, Takeya M, Ogawa H, et al. Co-localization of tissue factor and tissue factor pathway inhibitor in coronary atherosclerosis. J Pathol 1999;188:180–8.
[20] Crawley J, Lupu F, Westmuckett AD, et al. Expression, localization, and activity of tissue factor pathway inhibitor in normal and atherosclerotic human vessels. Arterioscler Thromb Vasc Biol 2000;20:1362–73.
[21] Kamikura Y, Wada H, Yamada A, et al. Increased tissue factor pathway inhibitor in patients with acute myocardial infarction. Am J Hematol 1997;55:183–7.
[22] Soejima H, Ogawa H, Yasue H, et al. Heightened tissue factor associated with tissue factor pathway inhibitor and prognosis in patients with unstable angina. Circulation 1999;99:2908–13.
[23] Sakkinen PA, Cushman M, Psaty BM, et al. Correlates of antithrombin, protein C, protein S, and TFPI in a healthy elderly cohort. Thromb Haemost 1998;80:134–9.
[24] Kohler HP, Grant PJ. Plasminogen-activator inhibitor type 1 and coronary artery disease. N Engl J Med 2000;342:1792–801.
[25] Folsom AR. Hemostatic risk factors for atherothrombotic disease: an epidemiologic view. Thromb Haemost 2001;86:366–73.
[26] Eitzman DT, Westrick RJ, Xu Z, Tyson J, Ginsburg D. Plasminogen activator inhibitor-1 deficiency protects against atherosclerosis progression in the mouse carotid artery. Blood 2000;96:4212–5.
[27] Hasenstab D, Lea H, Clowes AW. Local plasminogen activator inhibitor type 1 overexpression in rat carotid artery enhances thrombosis and endothelial regeneration while inhibiting intimal thickening. Arterioscler Thromb Vasc Biol 2000;20:853–9.
[28] Eren M, Painter CA, Atkinson JB, Declerck PJ, Vaughan DE. Age-dependent spontaneous coronary arterial thrombosis in transgenic mice that express a stable form of human plasminogen activator inhibitor-1. Circulation 2002;106:491–6.
[29] Tomiyama H, Kimura Y, Mitsuhashi H, et al. Relationship between endothelial function and fibrinolysis in early hypertension. Hypertension 1998;31:321–7.
[30] Kaikita K, Fogo AB, Ma L, et al. Plasminogen activator inhibitor-1 deficiency prevents hypertension and vascular fibrosis in response to long-term nitric oxide synthase inhibition. Circulation 2001;104:839–44.

MOLECULAR AND CELLULAR BIOLOGY, May 2004, p. 3949–3956 Vol. 24, No. 9
0270-7306/04/$08.00+0 DOI: 10.1128/MCB.24.9.3949–3956.2004

Ndrg1-Deficient Mice Exhibit a Progressive Demyelinating Disorder of Peripheral Nerves

Tomohiko Okuda,[1] Yujiro Higashi,[2] Koichi Kokame,[1] Chihiro Tanaka,[1] Hisato Kondoh,[2] and Toshiyuki Miyata[1]*

National Cardiovascular Center Research Institute, Suita, Osaka 565-8565,[1] and Laboratory of Developmental Biology, Graduate School of Frontier Bioscience, Osaka University, Suita, Osaka 565-0871,[2] Japan

Received 28 August 2003/Returned for modification 3 November 2003/Accepted 10 January 2004

NDRG1 is an intracellular protein that is induced under a number of stress and pathological conditions, and it is thought to be associated with cell growth and differentiation. Recently, human *NDRG1* was identified as a gene responsible for hereditary motor and sensory neuropathy-Lom (classified as Charcot-Marie-Tooth disease type 4D), which is characterized by early-onset peripheral neuropathy, leading to severe disability in adulthood. In this study, we generated mice lacking *Ndrg1* to analyze its function and elucidate the pathogenesis of Charcot-Marie-Tooth disease type 4D. Histological analysis showed that the sciatic nerve of *Ndrg1*-deficient mice degenerated with demyelination at about 5 weeks of age. However, myelination of Schwann cells in the sciatic nerve was normal for 2 weeks after birth. *Ndrg1*-deficient mice showed muscle weakness, especially in the hind limbs, but complicated motor skills were retained. In wild-type mice, NDRG1 was abundantly expressed in the cytoplasm of Schwann cells rather than the myelin sheath. These results indicate that NDRG1 deficiency leads to Schwann cell dysfunction, suggesting that NDRG1 is essential for maintenance of the myelin sheaths in peripheral nerves. These mice will be used for future analyses of the mechanisms of myelin maintenance.

NDRG1, an intracellular protein composed of 394 amino acids, is highly conserved among multicellular organisms, and its expression is induced by stress stimuli. Previously, we showed that NDRG1 is induced by homocysteine, 2-mercaptoethanol, and tunicamycin in cultured human endothelial cells (13). This pattern is similar to that seen for molecular chaperones in the endoplasmic reticulum. Subsequently, NDRG1 was found to be upregulated in a human lung cells following treatment with nickel compounds (31). This change in expression reflected an increase in hypoxia-inducible factor 1 caused by hypoxia or the subsequent elevation of intercellular calcium concentrations (23, 24). NDRG1 expression is also induced by p53 expression and DNA damage, and its expression is inhibited under conditions of cell growth (14). These results suggest that NDRG1 is involved in the cellular stress response mechanisms.

Conversely, *Ndrg1* was also identified as a downstream target of N-*myc* (25). In N-*myc* knockout mouse embryos, NDRG1 expression is upregulated. During the early stages of differentiation of some tissues, it seems that N-myc activity leads to decreased NDRG1 expression as tissue differentiation progresses. Indeed, *NDRG1* has been identified as a gene whose expression is downregulated in tumors (14, 27). Furthermore, NDRG1 expression is induced by differentiation stimuli in cancer cells (21, 29). *NDRG1* was also reported to be a metastasis suppressor gene (3, 6). In this regard, the effects of *NDRG1* are thought to reflect its potential role in cell differentiation.

Recently, a nonsense mutation of human *NDRG1* was reported to be causative for hereditary motor and sensory neuropathy-Lom (9), which is a severe peripheral neuropathy identified in the Gypsy community of Lom, a small town in northwest Bulgaria (10, 11). The hereditary motor and sensory neuropathy-Lom is classified as Charcot-Marie-Tooth disease type 4D (4). Patients with this disease exhibit an early-onset peripheral neuropathy that progresses to severe disability in adulthood, characterized by muscle weakness, sensory loss, and neural deafness. These symptoms are caused by demyelination of peripheral nerves. These observations suggest that NDRG1 is necessary for axonal survival.

To clarify the function(s) of NDRG1, we generated *Ndrg1*-deficient mice by gene targeting. The *Ndrg1*-deficient mice exhibited progressive demyelination in peripheral nerves. Moreover, we showed that NDRG1 was significantly expressed in the cytoplasm of Schwann cells, suggesting that NDRG1 deficiency is a primary cause of Schwann cell dysfunction.

MATERIALS AND METHODS

Construction of targeting vector. We isolated genomic clones carrying the mouse *Ndrg1* gene and characterized the promoter and the first exon (25). An 8.9-kb EcoRI fragment encompassing the promoter and exon 1 was used to construct the targeting vector. The initiating Met codon for NDRG1 translation exists in exon 2. A *loxP*-flanked pSTneoB (26) cassette was inserted at the BamHI site 1.2 kb downstream of the transcriptional start site, and an additional *loxP* plus BamHI site sequence was inserted at an EcoRV site 1.2 kb upstream of the start site. This resulted in three *loxP* sites in the vector, so that the Cre recombinase should excise the promoter and exon 1 (Fig. 1A). The sequence was inserted into the diphtheria toxin A fragment cassette vector (30), and the DNA was linearized by SalI digestion for electroporation.

* Corresponding author. Mailing address: National Cardiovascular Center Research Institute, 5-7-1 Fujishirodai, Suita, Osaka 565-8565, Japan. Phone: 81-6-6833-5012, ext. 2512. Fax: 81-6-6835-1176. E-mail: miyata@ri.ncvc.go.jp.

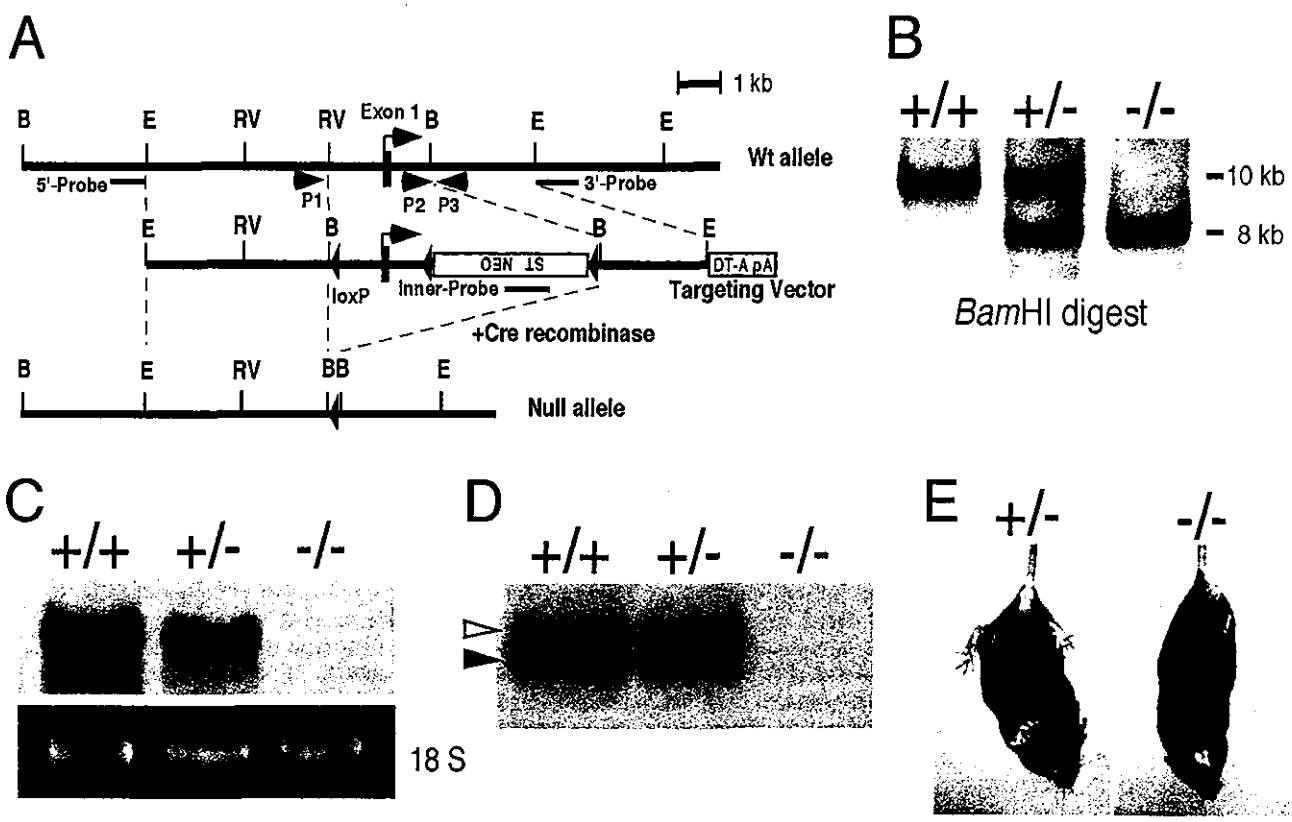

FIG. 1. Targeted disruption of *Ndrg1*. (A) Targeting strategy for the *Ndrg1* gene. Solid boxes represent exon 1 of *Ndrg1*. Arrowheads indicate the location and orientation of *loxP* sites. The *loxP*-flanked pSTneoB cassette (ST NEO) and the third *loxP* sequence were inserted into the targeting vector. A diphtheria toxin A fragment cassette with a polyadenylation signal (DT-A pA) was included at the 3′ end of the vector for negative selection of ES cells. 5′-External, 3′-external, and inner probes for selection of ES clones by Southern blotting are shown as bars. PCR primers to discriminate each allele are shown as P1, P2, and P3. B, BamHI; E, EcoRI; RV, EcoRV. (B) Southern blot analysis. Genomic DNA was prepared from littermates obtained by heterozygous intercrossing and subjected to BamHI digestion. The wild-type and null alleles gave about 10- and 8-kb bands, respectively, with the 5′ probe. (C) Northern blot analysis of the kidneys from 2-month-old male mice. The partial mouse *Ndrg1* cDNA fragment (904 bp) was used as a specific probe. Equal loading among lanes was confirmed by staining of 18 S rRNA. *Ndrg1* mRNA expression was not detected in $Ndrg1^{-/-}$ mice. (D) Western blot analysis of the kidneys from 2-month-old male mice. Each lane contains 5 μg of total protein. NDRG1 expression was partially reduced in the $Ndrg1^{+/-}$ mouse and absent in the $Ndrg1^{-/-}$ mouse. The majority of NDRG1 was detected at an apparent molecular mass of 43 kDa (solid arrowhead). The upper bands indicate phosphorylated NDRG1 (open arrowhead). (E) A phenotype in the appearance of an $Ndrg1^{-/-}$ mouse at 3 months of age. An abnormal hind limb clasping phenotype was seen in $Ndrg1^{-/-}$ mice upon tail suspension, indicating neurological abnormalities.

Generation of *Ndrg1*-null mutant mice. R1 embryonic stem (ES) cells (18) were electroporated with the targeting vector and selected with 250 μg of G418 per ml. G418-resistant ES colonies were selected, and correctly targeted clones were identified by Southern blotting with a Gene Images Random-Prime system (Amersham Biosciences) with 5′-external, 3′-external, and inner probes (Fig. 1A). These ES cells were injected into blastocysts to obtain mouse chimeras, which were crossed with wild-type C57BL/6 mice (SLC Japan) for germ line transmission of the floxed *Ndrg1* allele. These mice were further crossed with *EIIa-Cre* deleter mice (15) to excise the promoter and exon 1 region of the *Ndrg1* gene together with the neomycin resistance cassette (7). Successful excision of the sequences in the offspring was confirmed by PCR analysis of DNA isolated from punctured ear lobes with primers P1 (5′-AGCAGGCTCTTAAAGCGGC TCC-3′), P2 (5′-CCGCCTCTGTCAAATTAGTAGCTG-3′), and P3 (5′-GGG AGAGCTGAAGGCTGTTCTAGG-3′). Those heterozygous mice with the excised *Ndrg1* allele were backcrossed with wild-type C57BL/6 mice. The heterozygous offspring lacking the *Cre* gene were used for this study. The experiments were conducted in accordance with the current guidelines for the care and use of experimental animals of the National Cardiovascular Center in Japan.

Northern blot analysis. Male mice aged 2 months (wild-type, heterozygous, and homozygous mice) were sacrificed, and their kidneys and sciatic nerves were excised. For extraction of total RNA, whole kidneys or sciatic nerves were immediately homogenized in Trizol reagent (Invitrogen). Isolated total RNA was electrophoresed in a 1% agarose gel containing 2% formaldehyde (10 μg/lane) and transferred to a nylon membrane. To make a specific probe, a partial cDNA fragment (904 bp) was amplified by PCR with primers 5′-CTCAGACA CCAAACTGCCAAAAC-3′ and 5′-AATGCTACAAACCCAGTCAGCAG-3′, with the full-length *Ndrg1* cDNA used as a template. The fragment obtained was labeled with fluorescein-12-dUTP (PerkinElmer Life Sciences), and hybridization and detection procedures were performed as previously described (32).

Western blot analysis. For extraction of total protein, the excised organs were homogenized in lysis buffer as described before (12). The protein lysates were subjected to sodium dodecyl sulfate-polyacrylamide gel electrophoresis (10 to 20% gradient gel) and transferred to a polyvinylidene difluoride membrane (Bio-Rad). After blocking with 3% skim milk in phosphate-buffered saline (PBS) with 0.05% Tween 20, the membrane was incubated with a 1:1,000 dilution of anti-NDRG1 antiserum (2) and then with a 1:1,000 dilution of peroxidase-conjugated goat anti-rabbit immunoglobulin G (Zymed). Detection was performed with the Western Lightning Chemiluminescence Reagent Plus (PerkinElmer Life Sciences) with the LAS-1000plus image analyzer.

Histological analyses. Male mice aged 1, 2, and 5 weeks and 3 and 6 months (wild-type, heterozygous, and homozygous mice) were anesthetized with nembutal (Abbott Laboratories) and perfused with ice-cold PBS containing 4% paraformaldehyde, and sciatic nerve fragments were excised. For light and electron microscopy, the fragments were fixed with 2.5% glutaraldehyde for 2 h at 4°C. After being washed with PBS, the samples were cut into small pieces and fixed with 2% OsO_4 for 2 h at 4°C. After dehydration in an ascending ethanol series, the samples were embedded in Quetol812 resin. For light microscopy, semithin sections (1-μm thickness) of sciatic nerves were stained with 0.1%

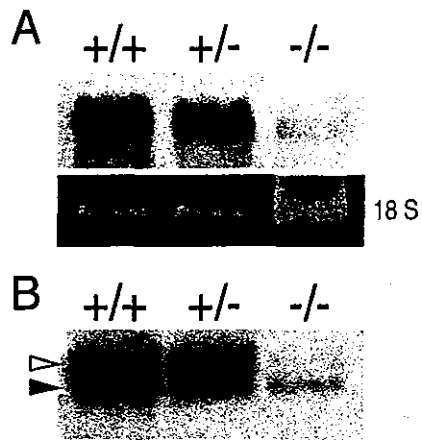

FIG. 2. Leaky expression of NDRG1 in the sciatic nerve of *Ndrg1*$^{-/-}$ mice. (A) Northern blot analysis of the sciatic nerves from mice at 2 months of age. 18 S rRNA was used as an internal control. (B) Western blot analysis of the sciatic nerves from mice at 2 months of age. Each lane contains 5 μg of total protein. NDRG1 was detected at 43 kDa (solid arrowhead). The upper bands indicate phosphorylated NDRG1 (open arrowhead). Low-level expression of NDRG1 was detected in the sciatic nerves of *Ndrg1*$^{-/-}$ mice.

toluidine blue. Slides were examined with an Axioplan 2 microscope (Carl Zeiss). For electron microscopy, ultrathin sections (90-nm thickness) on mesh grids were stained with uranyl acetate and lead acetate and examined with an H-300 electron microscope (Hitachi).

For immunofluorescence microscopy, paraformaldehyde-fixed sciatic nerve specimens from mice aged 3 weeks (wild-type and homozygous mice) were washed with PBS at 4°C and embedded in OCT compound (Sakura Finetek) at −80°C. Frozen sections (5-μm thickness) were washed with PBS. After being blocked with 10% normal goat serum for 15 min at room temperature, the sections were incubated with a 1:200 dilution of anti-NDRG1 antiserum and a 1:100 dilution of rat anti-myelin basic protein (MBP) monoclonal antibody (Chemicon) overnight at 4°C and then with a 1:100 dilution of Alexa Fluor 488-conjugated anti-rabbit immunoglobulin G antibody (Molecular Probes) and a 1:100 dilution of Alexa Fluor 546-conjugated anti-rat immunoglobulin G antibody (Molecular Probes) for 1 h at room temperature. Fluorescence was detected with the Axiovert 200 microscope and photographed with the AxioCam (Carl Zeiss).

Quantitative analysis of demyelination. Semithin sections of sciatic nerves from three homozygous and three wild-type mice aged 3 weeks and 3 months were photographed, and myelinated axons in a fixed area were counted manually. The diameter of the axons and the thickness of nerve fibers (axon plus myelin) were analyzed with ImageGauge software (Fujifilm). To assess the thickness of the myelin sheath, the g ratio (axon diameter/fiber diameter) was calculated (1, 5). Complex figures with folded myelin were excluded. The significance of differences between mean values was determined by the *F* test.

RT-PCR analysis. Total RNA was extracted from the sciatic nerves, kidneys, and brains of homozygous and wild-type mice aged 5 weeks. Reverse transcription-PCR (RT-PCR) was performed with total RNA (50 ng) as the template and a SuperScript One-Step RT-PCR kit with Platinum *Taq* (Invitrogen). The primer pairs were 5′-ACCCTGAGATGGTAGAGGGTCTC-3′ and 5′-CCAATTTAG AATTGCATTCCACC-3′ for *Ndrg1*, 5′-ATTCTTGGACATCTTTTCAGCC A-3′ and 5′-TGCAGGAAGTACTTGAAAGCCTC-3′ for *Ndrg2*, 5′-CATTAA CATTGACCCGTGTGCTA-3′ and 5′-TTGTATTTATAGGGTCGAGGCG A-3′ for *Ndrg3*, 5′-AAGTACGTGATTGGCATTGGAGT-3′ and 5′-CAGGTG CATTATCTCCGACTACC-3′ for *Ndrg4*, and 5′-GGAGAAACCTGCCAAGT ATGATG-3′ and 5′-CTAGGCCCCTCCTGTTATTATGG-3′ for *Gapd*.

Motor activity tests. In the wire-hanging test, we assessed the grip strength of the mice as described before (8). Each mouse was placed on wire netting (20 by 30 cm) taped around the edge. The wire netting was shaken three times and turned upside down. The amount of time that each mouse held onto the wire netting was recorded up to a maximum of 300 s. In the rotorod test, we assessed the ability of the mice to maintain balance on a rotating cylinder as described before (17). The accelerating Rota-Rod (model 7650; Ugo Basile) consists of a 3-cm-diameter cylinder with knurls. Each mouse was placed on the cylinder, which turned at a constant rotation (5 rpm) for 1 min for training, and then the

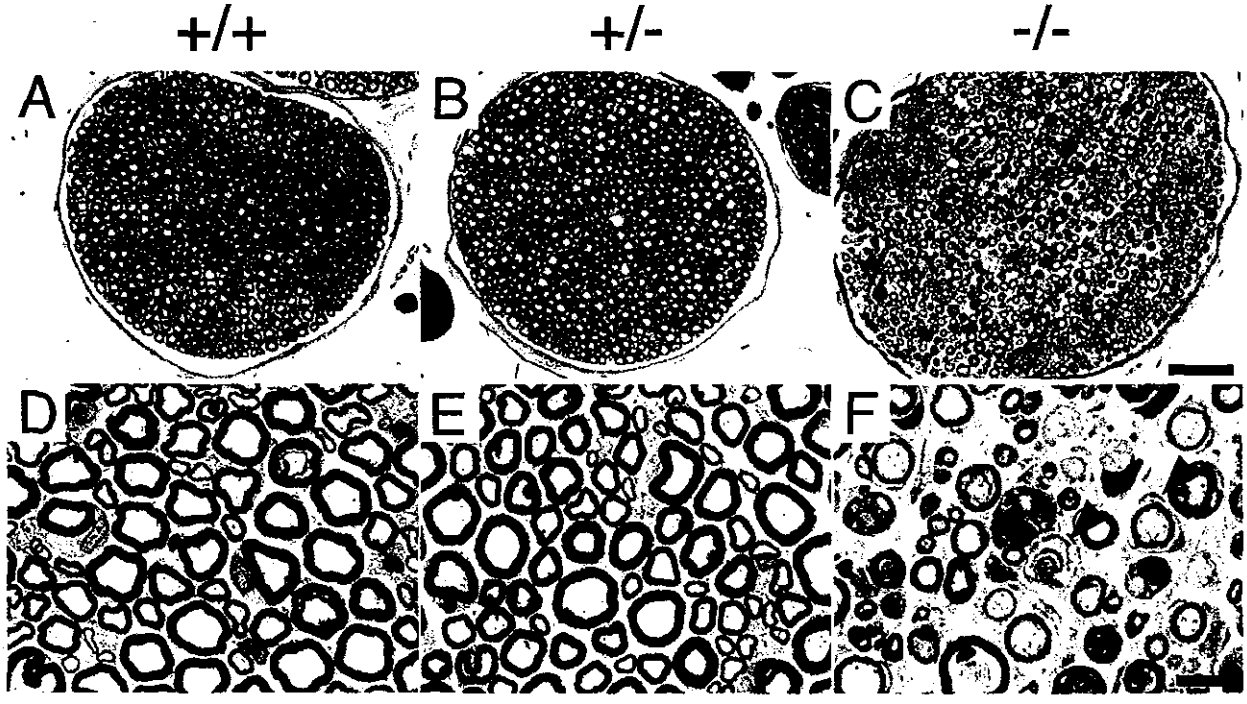

FIG. 3. Histological examination of sciatic nerves. Transverse sections of the sciatic nerves from *Ndrg1*$^{+/+}$ (A and D), *Ndrg1*$^{+/-}$ (B and E), and *Ndrg1*$^{-/-}$ (C and F) mice at 3 months of age are shown. Panels D, E, and F are higher magnifications of panels A, B, and C, respectively. The sciatic nerves of the *Ndrg1*$^{-/-}$ mouse (C and F) showed features typical of demyelinating neuropathy. Many thinly myelinated axons and onion bulb degeneration were seen (arrowheads). No difference was observed between *Ndrg1*$^{+/+}$ and *Ndrg1*$^{+/-}$ mice. Bars, 50 μm (A to C); 10 μm (D to F).

TABLE 1. Quantitative analysis of sciatic nerve[a]

Age	*Ndrg1* genotype	Mean axon density (10^4/mm^2) ± SD	Mean axon diam (μm) ± SD	Mean g ratio ± SD (no. of fibers)
3 wk	+/+	2.65 ± 0.23	3.46 ± 0.97	0.67 ± 0.06 (980)
	−/−	2.87 ± 0.22	3.09 ± 0.82*	0.66 ± 0.06 (1,028)
3 mo	+/+	2.45 ± 0.32	4.13 ± 1.41	0.67 ± 0.06 (760)
	−/−	1.61 ± 0.12*	3.19 ± 1.09*	0.73 ± 0.09* (661)

[a] *, statistically different from *Ndrg1*$^{+/+}$ mice of the same age ($P < 0.05$).

rotation speed was increased over a 300-s period from 5 to 30 rpm. The amount of time that the mouse remained on the accelerating cylinder was recorded. Mice that fell in less than 15 s were given a second trial. Mice that did not fall during the 300-s trial period were given a score of 300 s. Two sets of the rotorod test were performed in the same day, and the higher score for each mouse is reported. The body weight of each mouse was also measured. Both motor activity tests were carried out once every 2 weeks from 5 to 19 weeks of age.

RESULTS

Generation of *Ndrg1*-deficient mice. We made a targeting vector to eliminate *Ndrg1* expression by deletion of the promoter and exon 1 region with *Cre-loxP* excision (Fig. 1A). R1 ES cells were electroporated with the targeting vector and selected with G418. One hundred forty-five G418-resistant ES colonies were selected, and correctly targeted clones were identified by Southern blotting with a 5′-external sequence probe (Fig. 1A and B). Five independently targeted clones were isolated, and the genomic organization of their *Ndrg1* locus was further confirmed by Southern blotting with 3′-external and internal probes. After *Cre-loxP* excision, two lines of mice heterozygous for deletion of the *Ndrg1* promoter and exon 1 were obtained. Mice with the deleted *Ndrg1* allele and without the *Cre* gene (*Ndrg1*$^{+/-}$) were backcrossed with wild-type C57BL/6 mice (*Ndrg1*$^{+/+}$). The *Ndrg1*$^{+/-}$ mice were crossed to generate homozygous *Ndrg1*-deficient mice (*Ndrg1*$^{-/-}$).

Phenotype of *Ndrg1*-deficient mice. *Ndrg1*$^{-/-}$ mice were born normally with the expected Mendelian frequency. Both male and female *Ndrg1*$^{-/-}$ mice were fertile. We confirmed the elimination of NDRG1 expression in the kidney, where NDRG1 was abundantly expressed in wild-type mice (Fig. 1C and D) (32). However, in the sciatic nerve, a faint signal of *Ndrg1* mRNA was detectable in *Ndrg1*$^{-/-}$ mice by Northern blot analysis (Fig. 2A). Leaky transcription of NDRG1 might be possible because the *Ndrg1*$^{-/-}$ mice still showed normal organization of the *Ndrg1* gene downstream of exon 2, containing the initiating Met codon. To confirm this possibility, we performed Western blot analysis on lysates from the sciatic nerves of *Ndrg1*$^{+/+}$, *Ndrg1*$^{+/-}$, and *Ndrg1*$^{-/-}$ mice. As shown in Fig. 2B, faint bands corresponding to the normal size of NDRG1 were observed. These data suggested that a small amount of full-length NDRG1 was expressed in the sciatic nerves of *Ndrg1*$^{-/-}$ mice. In this regard, *Ndrg1*$^{-/-}$ mice are hypomorphic, at least in the sciatic nerves.

Despite the low-level expression of NDRG1, *Ndrg1*$^{-/-}$ mice began showing hind limb weakness at 3 months of age. We also detected an abnormal limb clasping phenotype in *Ndrg1*$^{-/-}$ mice upon tail suspension (Fig. 1E). These observations suggested neurological abnormalities. These phenotypes were progressive, that is, 1-year-old or older *Ndrg1*$^{-/-}$ mice exhibited substantial impairment in hind limb function (i.e., dragging of their legs) and leg muscle atrophy. Two independent lines of *Ndrg1*$^{-/-}$ mice exhibited similar phenotypes. *Ndrg1*$^{+/-}$ mice were indistinguishable from *Ndrg1*$^{+/+}$ mice in both appearance and behavior.

Peripheral nerve degeneration of *Ndrg1*-deficient mice. To address possible peripheral nerve dysfunction, we performed histological analyses. Severe degeneration of the sciatic nerves in *Ndrg1*$^{-/-}$ mice was seen at 3 months of age. We observed a large number of thinly myelinated axons (Fig. 3C and F). The myelinated axons were significantly decreased in density, and the g ratios of the neuronal fibers were significantly increased in *Ndrg1*$^{-/-}$ mice at 3 months of age (Table 1). Electron microscopy of the sciatic nerve showed onion bulb pathology with Schwann cell processes, thin myelin sheaths, endoneurial collagenization, and infiltration of macrophages in *Ndrg1*$^{-/-}$ mice (Fig. 4C). A similar demyelinating phenotype is seen in human Charcot-Marie-Tooth disease type 4D patients (11).

To investigate the process of demyelination in *Ndrg1*$^{-/-}$ mice, we assessed the initial formation of the neuronal myelin sheath at a younger age. Histological analysis showed that, at 1 and 2 weeks of age, the sciatic nerves of *Ndrg1*$^{-/-}$ mice did not differ from the nerves of *Ndrg1*$^{+/+}$ mice; both displayed normal

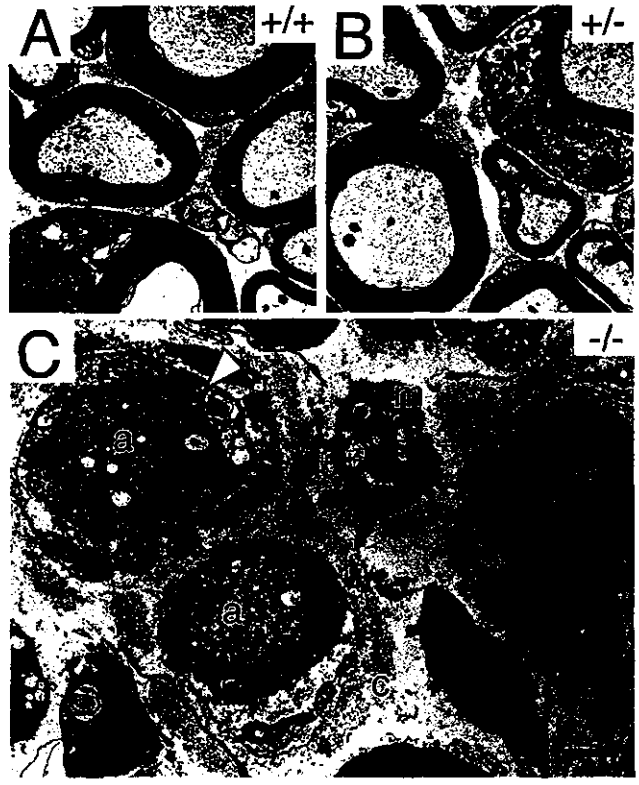

FIG. 4. Electron microscopy of sciatic nerves. Electron micrographs of the sciatic nerves from *Ndrg1*$^{+/+}$ (A), *Ndrg1*$^{+/-}$ (B), and *Ndrg1*$^{-/-}$ (C) mice at 3 months of age were shown. Onion bulb pathology with Schwann cell processes (*open arrowhead*), axons with thin myelin sheath (a), excess collagenization (c), and infiltration of macrophages (m) were observed in *Ndrg1*$^{-/-}$ mice. Bar, 2 μm.

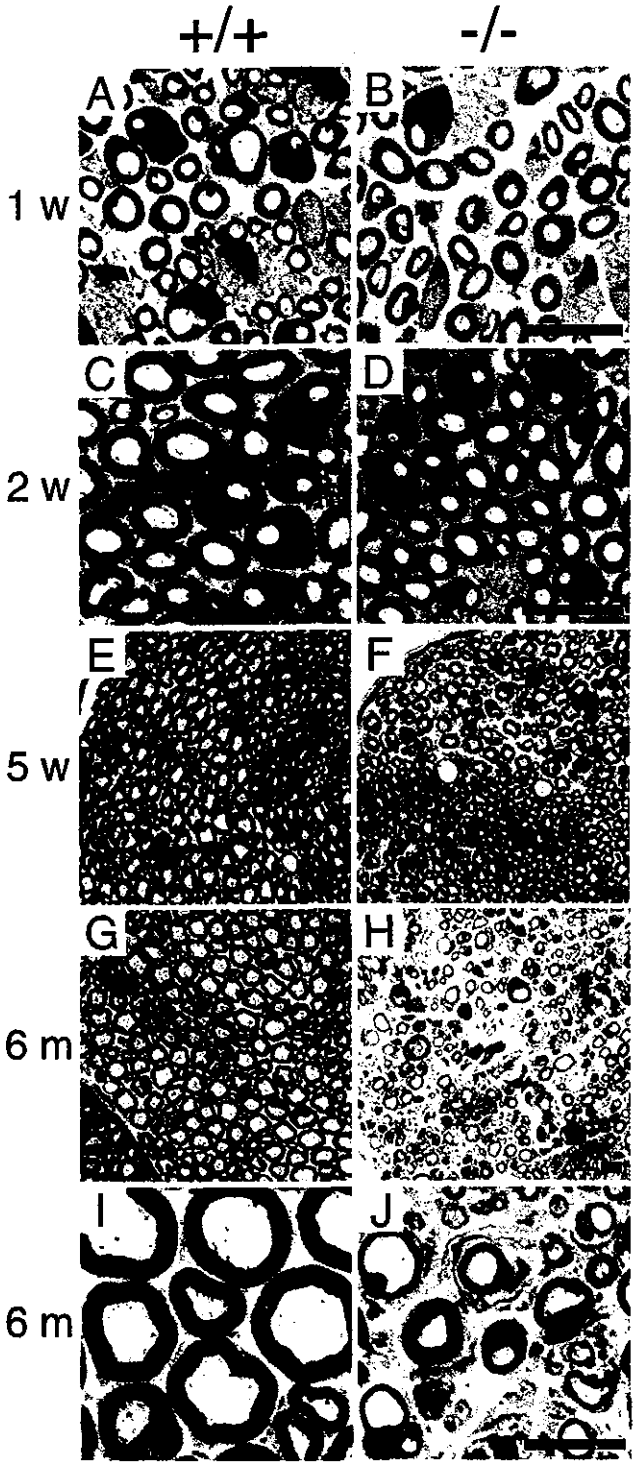

FIG. 5. Time course analysis of sciatic nerves during growth. Transverse sections of the sciatic nerves from *Ndrg1*$^{+/+}$ (A, C, E, G, and I) and *Ndrg1*$^{-/-}$ (B, D, F, H, and J) mice were compared. These specimens were derived from mice of the following ages: A and B, 1 week; C and D, 2 weeks; E and F, 5 weeks; and G to J, 6 months. Panels I and J are higher magnifications of panels G and H, respectively. At 1 to 2 weeks of age, Schwann cell proliferation and myelin formation were normal, and no demyelination was observed in *Ndrg1*$^{-/-}$ mice. However, at 5 weeks of age, partial degeneration of the sciatic nerves had occurred in *Ndrg1*$^{-/-}$ mice, especially in relatively thick axons. At 6 months of age, degeneration of the sciatic nerves had progressed further, with an apparent reduction of myelinated axons in *Ndrg1*$^{-/-}$ mice. Bars, 10 μm.

growth of Schwann cells and normal formation of the myelin sheath (Fig. 5A to D). At 3 weeks of age, the density of myelinated axons was not affected in *Ndrg1*$^{-/-}$ mice, and no significant difference in the g ratios was observed (Table 1). However, at 5 weeks of age, the myelin sheaths of *Ndrg1*-deficient mice began to degenerate (Fig. 5F). The observed demyelination was incomplete and sporadic but was especially pronounced in the myelin sheaths of relatively thick axons. These results indicated that Schwann cell proliferation and myelination were normal and that some defect in the maintenance of the myelin sheath occurred in *Ndrg1*$^{-/-}$ mice. Older *Ndrg1*$^{-/-}$ mice exhibited more severe disease in their sciatic nerves, demonstrating that this peripheral nerve degeneration is progressive (Fig. 5G to J).

NDRG1 is ubiquitously expressed in various tissues (13, 32). In particular, the kidney is reported to be a site of high NDRG1 expression in mice and humans (16, 32). Although the peripheral nerves of *Ndrg1*$^{-/-}$ mice demonstrated clear pathology, no apparent morphological abnormality was observed in their kidneys (data not shown).

Localization of NDRG1 protein in the sciatic nerve. To examine which cells, neurons or Schwann cells, are responsible for the demyelinating defects, we investigated the expression of NDRG1 in the sciatic nerve by immunohistochemical analysis. At 3 weeks of age, NDRG1 was abundantly expressed in the cytoplasm of Schwann cells rather than in myelin sheaths or axons in *Ndrg1*$^{+/+}$ mice (Fig. 6A to C). We confirmed that MBP, a myelin marker protein, was normally expressed in the myelin sheath of the sciatic nerves of both *Ndrg1*$^{+/+}$ and *Ndrg1*$^{-/-}$ mice (Fig. 6B and E). These results suggested that the cytoplasmic expression of NDRG1 in Schwann cells is essential for the maintenance of myelin structure. Thus, defects in Schwann cells caused by NDRG1 deficiency could be a primary cause of the neural degeneration seen in *Ndrg1*$^{-/-}$ mice.

Expression of other NDRG family members. To compare the expression patterns of all NDRG family members, we performed RT-PCR analysis on RNA samples from the sciatic nerve, brain, and kidney of *Ndrg1*$^{+/+}$ and *Ndrg1*$^{-/-}$ mice (Fig. 7). In *Ndrg1*$^{+/+}$ mice, *Ndrg1* was expressed in the sciatic nerves as much as in the kidney but relatively less expressed in the brain. In contrast, *Ndrg2*, *Ndrg3*, and *Ndrg4* were abundantly expressed in the brain of both *Ndrg1*$^{+/+}$ and *Ndrg1*$^{-/-}$ mice but less in the sciatic nerves. Upregulation of *Ndrg2*, *Ndrg3*, and *Ndrg4* was not observed in *Ndrg1*$^{-/-}$ mice.

Muscle strength and motor activity of *Ndrg1*-deficient mice. To examine the muscle strength of the legs, the wire-hanging test was performed. *Ndrg1*$^{-/-}$ mice were able to hang onto the wire for a significantly shorter period than *Ndrg1*$^{+/+}$ at all ages tested. *Ndrg1*$^{-/-}$ mice demonstrated that their muscle strength was quite decreased. Male mice of both genotypes tended to fall sooner than females due to their heavier body weight (Fig. 8A and C). To measure more complicated motor activities and motor learning in the same mice, a rotorod test was carried out. The scores of older *Ndrg1*$^{-/-}$ mice in this test were slightly lower than those of the age-matched *Ndrg1*$^{+/+}$ controls, though the differences were minor compared to those seen in the wire-hanging test (Fig. 8B).

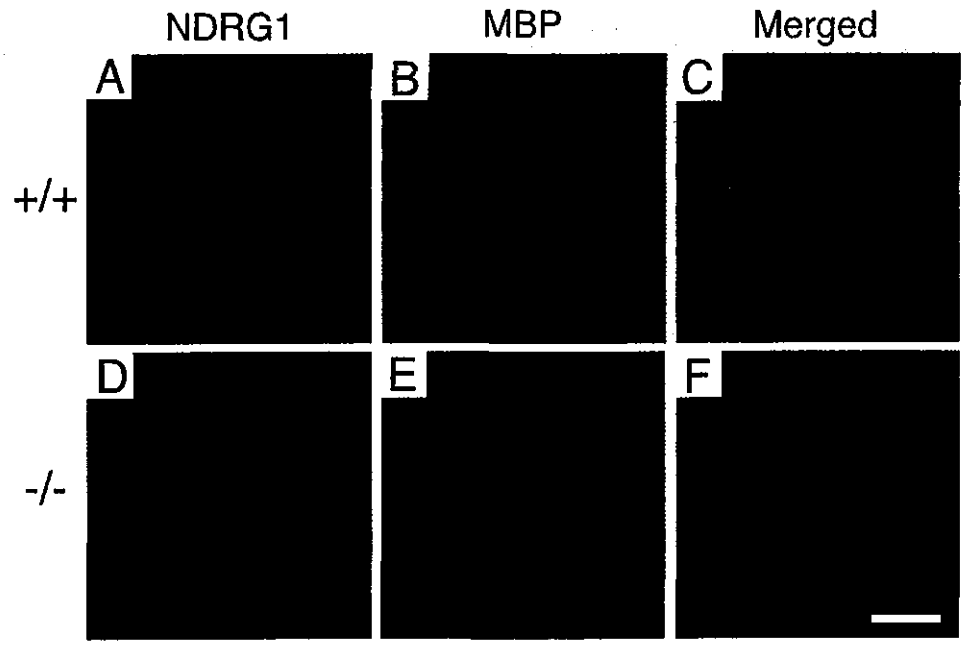

FIG. 6. Immunofluorescence analysis of sciatic nerves. Transverse sections of the sciatic nerves from mice at 3 weeks of age were double stained with anti-NDRG1 antiserum (green; A and D) and anti-MBP antibody (red; B and E). Sections from *Ndrg1*$^{+/+}$ (A to C) and *Ndrg1*$^{-/-}$ (D to F) mice were compared. The merged images are shown in panels C and F. Bar, 10 μm.

DISCUSSION

In this study, we successfully generated *Ndrg1*$^{-/-}$ mice. The *Ndrg1*$^{-/-}$ mice exhibited a progressive demyelinating disorder of the peripheral nerves. Histological and quantitative analyses revealed that Schwann cell proliferation and the initial myelination of *Ndrg1*$^{-/-}$ mice were normal after birth (Fig. 5 and Table 1). However, sporadic degeneration began by 5 weeks of age (Fig. 5). These results strongly suggest that the ability to form myelin sheaths is retained but some defect in the maintenance of the myelin sheath is present in the Schwann cells of *Ndrg1*$^{-/-}$ mice. Therefore, NDRG1 is essential for maintenance of the myelin sheath.

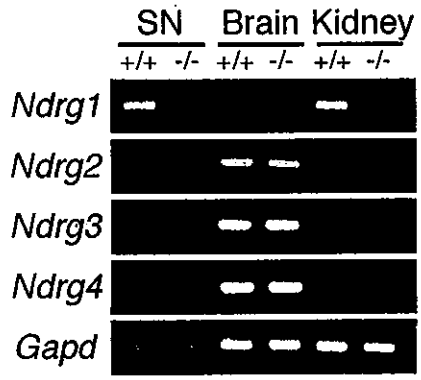

FIG. 7. mRNA expression of *Ndrg* family members. RT-PCR analysis was performed on total RNA samples from the sciatic nerves, brains, and kidneys of *Ndrg1*$^{+/+}$ and *Ndrg1*$^{-/-}$ mice at 5 weeks of age. In *Ndrg1*$^{+/+}$ mice, *Ndrg1* was expressed in the sciatic nerve as much as in the kidney. In contrast, *Ndrg2*, *Ndrg3*, and *Ndrg4* were abundantly expressed in the brain but less in the sciatic nerve. Expression of *Gapd* was examined as an internal control. SN, sciatic nerve.

It has been reported that NDRG1 expression is induced by differentiation or stress stimuli (21, 27, 29). NDRG1 has also been proposed to shuttle between the cytoplasm and the nucleus in cells (14). Furthermore, phosphorylation of NDRG1 depends on extracellular stimuli (2). These observations imply that NDRG1 may have a role in signal transduction. Recently, it was reported that rat NDRG1 is expressed in astrocytes only in the regions where neurons existed (28). This observation suggests that NDRG1 may also play a similar role in neuronal survival in the brain. We demonstrated that NDRG1 was abundantly expressed in the Schwann cell cytoplasm rather than in myelin sheaths (Fig. 6). This expression pattern is unique compared to that of other Charcot-Marie-Tooth disease-responsible proteins, such as peripheral myelin protein 22, myelin protein zero, connexin 32, and L-periaxin (4). These proteins are localized to the plasma membrane of Schwann cells and are thought to have a role in the formation and/or stabilization of the myelin sheaths. Cytoplasmic expression and phosphorylation of NDRG1 implies its association with intracellular signal transduction in Schwann cells. The NDRG1-mediated signals in Schwann cells related to axonal cross talk could be important for the maintenance of myelin sheaths and axonal survival.

Ndrg1$^{-/-}$ mice exhibited muscle weakness, whereas the complicated motor abilities were relatively retained (Fig. 8). These results indicate that NDRG1 deficiency causes peripheral nerve degeneration leading to muscle weakness. This suggests that peripheral nerves may be quite vulnerable to NDRG1 deficiency but that some degree of functional redundancy for NDRG1 may exist within the central nervous system. NDRG1 is one of four NDRG family members exhibiting different expression patterns (20, 22, 32). We previously demonstrated that NDRG4 is abundantly expressed in neurons in the brain but not in the peripheral nerves (32). NDRG4 ex-

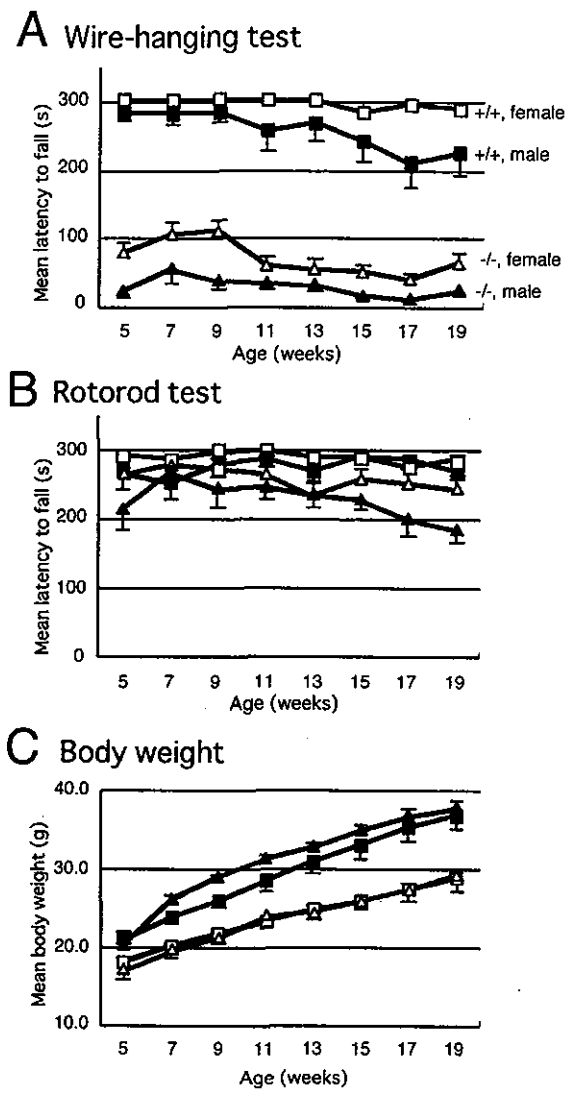

FIG. 8. Assessment of motor activity of *Ndrg1*$^{-/-}$ mice. (A) The wire-hanging test was carried out to measure the grip strength of *Ndrg1*$^{+/+}$ (seven males and seven females) and *Ndrg1*$^{-/-}$ (seven males and six females) mice. The time that each mouse held onto the wire netting was recorded up to a maximum of 300 s. The mean (± standard error of the mean) time before the mouse fell off is shown. (B) The rotorod test was carried out to measure more complicated motor activities in the same mice. The time that each mouse held onto the accelerating cylinder was recorded up to a maximum of 300 s. Mean (±standard error of the mean) time before the mouse fell off the cylinder is shown. Although *Ndrg1*$^{-/-}$ mice tended to fall sooner, the differences observed between *Ndrg1*$^{-/-}$ and *Ndrg1*$^{+/+}$ mice were less than those seen in the wire-hanging test. (C) Plot of body weights of the same mice. Mean (± standard error of the mean) body weights are shown. Each test was carried out on mice from 5 to 19 weeks of age.

pression is induced by homocysteine and reduced both the proliferation and migration rates of cultured cells (19), suggesting that NDRG4 could play a role similar to that of NDRG1 in the brain. NDRG2 and NDRG3 were expressed less in the sciatic nerve than in the brain (Fig. 7). Indeed, no apparent morphological abnormality of the brain was detected in *Ndrg1*$^{-/-}$ mice (data not shown). NDRG1 deficiency may be compensated for by other NDRG members in the brain.

Although the *Ndrg1*$^{-/-}$ mice exhibited reductive depletion of NDRG1, a nonsense mutation of human *NDRG1* (R148X) is responsible for Charcot-Marie-Tooth disease type 4D (9). The phenotypes of patients with this disease (10, 11) and of *Ndrg1*$^{-/-}$ mice in peripheral nerves were similar. This suggests that the C-terminal region of NDRG1 may be essential for NDRG1 function.

In conclusion, we found that NDRG1 deficiency leads to a peripheral neuropathy characterized by demyelination, though the initial formation of the myelin sheaths was normal. NDRG1 is abundantly expressed in the cytoplasm of Schwann cells and plays an essential role in maintenance of myelin sheaths. Although the exact molecular functions of NDRG1 are still under investigation, the *Ndrg1*$^{-/-}$ mouse will be a good model for Charcot-Marie-Tooth disease type 4D and may be used for future analysis of human peripheral nerve neuropathy as well as provide insight into potential therapies.

ACKNOWLEDGMENTS

We thank A. Nagy (Mt. Sinai Hospital) for providing R1 ES cells and *loxP* and *Cre* plasmids. We are grateful to H. Westphal (NIH) for the *EIIa-Cre* mice. We also thank Y. Imai (Riken BSI) for critical discussion.

This work was supported in part by grants-in-aid from the Ministry of Health, Labor, and Welfare of Japan and the Ministry of Education, Culture, Sports, Science, and Technology of Japan and by the Program for Promotion of Fundamental Studies in Health Science of the Organization for Pharmaceutical Safety and Research of Japan.

REFERENCES

1. **Adlkofer, K., R. Martini, A. Aguzzi, J. Zielasek, K. V. Toyka, and U. Suter.** 1995. Hypermyelination and demyelinating peripheral neuropathy in *Pmp22*-deficient mice. Nat. Genet. **11**:274–280.
2. **Agarwala, K. L., K. Kokame, H. Kato, and T. Miyata.** 2000. Phosphorylation of RTP, an ER stress-responsive cytoplasmic protein. Biochem. Biophys. Res. Commun. **272**:641–647.
3. **Bandyopadhyay, S., S. K. Pai, S. C. Gross, S. Hirota, S. Hosobe, K. Miura, K. Saito, T. Commes, S. Hayashi, M. Watabe, and K. Watabe.** 2003. The *Drg-1* gene suppresses tumor metastasis in prostate cancer. Cancer Res. **63**:1731–1736.
4. **Berger, P., P. Young, and U. Suter.** 2002. Molecular cell biology of Charcot-Marie-Tooth disease. Neurogenetics **4**:1–15.
5. **Bosboom, W. M., L. H. van den Berg, H. Franssen, P. C. Giesbergen, H. Z. Flach, A. M. van Putten, H. Veldman, and J. H. Wokke.** 2001. Diagnostic value of sural nerve demyelination in chronic inflammatory demyelinating polyneuropathy. Brain **124**:2427–2438.
6. **Guan, R. J., H. L. Ford, Y. Fu, Y. Li, L. M. Shaw, and A. B. Pardee.** 2000. Drg-1 as a differentiation-related, putative metastatic suppressor gene in human colon cancer. Cancer Res. **60**:749–755.
7. **Higashi, Y., M. Maruhashi, L. Nelles, T. Van de Putte, K. Verschueren, T. Miyoshi, A. Yoshimoto, H. Kondoh, and D. Huylebroeck.** 2002. Generation of the floxed allele of the *SIP1* (*Smad-interacting protein 1*) gene for Cre-mediated conditional knockout in the mouse. Genesis **32**:82–84.
8. **Hoogenraad, C. C., B. Koekkoek, A. Akhmanova, H. Krugers, B. Dortland, M. Miedema, A. van Alphen, W. M. Kistler, M. Jaegle, M. Koutsourakis, N. Van Camp, M. Verhoye, A. van der Linden, I. Kaverina, F. Grosveld, C. I. De Zeeuw, and N. Galjart.** 2002. Targeted mutation of *Cyln2* in the Williams syndrome critical region links CLIP-115 haploinsufficiency to neurodevelopmental abnormalities in mice. Nat. Genet. **32**:116–127.
9. **Kalaydjieva, L., D. Gresham, R. Gooding, L. Heather, F. Baas, R. de Jonge, K. Blechschmidt, D. Angelicheva, D. Chandler, P. Worsley, A. Rosenthal, R. H. King, and P. K.** 2000. Thomas. N-myc downstream-regulated gene 1 is mutated in hereditary motor and sensory neuropathy-Lom. Am. J. Hum. Genet. **67**:47–58.
10. **Kalaydjieva, L., J. Hallmayer, D. Chandler, A. Savov, A. Nikolova, D. Angelicheva, R. H. King, B. Ishpekova, K. Honeyman, F. Calafell, A. Shmarov, J. Petrova, I. Turnev, A. Hristova, M. Moskov, S. Stancheva, I. Petkova, A. H. Bittles, V. Georgieva, L. Middleton, and P. K. Thomas.** 1996. Gene mapping in Gypsies identifies a novel demyelinating neuropathy on chromosome 8q24. Nat. Genet. **14**:214–217.
11. **Kalaydjieva, L., A. Nikolova, I. Turnev, J. Petrova, A. Hristova, B. Ishpekova, I. Petkova, A. Shmarov, S. Stancheva, L. Middleton, L. Merlini, A. Trogu, J. R. Muddle, R. H. King, and P. K. Thomas.** 1998. Hereditary motor

and sensory neuropathy-Lom, a novel demyelinating neuropathy associated with deafness in gypsies. Clinical, electrophysiological and nerve biopsy findings. Brain 121:399–408.
12. **Kokame, K., K. L. Agarwala, H. Kato, and T. Miyata.** 2000. Herp, a new ubiquitin-like membrane protein induced by endoplasmic reticulum stress. J. Biol. Chem. 275:32846–32853.
13. **Kokame, K., H. Kato, and T. Miyata.** 1996. Homocysteine-respondent genes in vascular endothelial cells identified by differential display analysis. J. Biol. Chem. 271:29659–29665.
14. **Kurdistani, S. K., P. Arizti, C. L. Reimer, M. M. Sugrue, S. A. Aaronson, and S. W. Lee.** 1998. Inhibition of tumor cell growth by *RTP/rit42* and its responsiveness to p53 and DNA damage. Cancer Res. 58:4439–4444.
15. **Lakso, M., J. G. Pichel, J. R. Gorman, B. Sauer, Y. Okamoto, E. Lee, F. W. Alt, and H. Westphal.** 1996. Efficient in vivo manipulation of mouse genomic sequences at the zygote stage. Proc. Natl. Acad. Sci. USA 93:5860–5865.
16. **Lin, T. M., and C. Chang.** 1997. Cloning and characterization of *TDD5*, an androgen target gene that is differentially repressed by testosterone and dihydrotestosterone. Proc. Natl. Acad. Sci. USA 94:4988–4993.
17. **Liu, Y., A. Hoffmann, A. Grinberg, H. Westphal, M. P. McDonald, K. M. Miller, J. N. Crawley, K. Sandhoff, K. Suzuki, and R. L. Proia.** 1997. Mouse model of G_{M2} activator deficiency manifests cerebellar pathology and motor impairment. Proc. Natl. Acad. Sci. USA 94:8138–8143.
18. **Nagy, A., J. Rossant, R. Nagy, W. Abramow-Newerly, and J. C. Roder.** 1993. Derivation of completely *cell culture*-derived mice from early-passage embryonic stem cells. Proc. Natl. Acad. Sci. USA 90:8424–8428.
19. **Nishimoto, S., J. Tawara, H. Toyoda, K. Kitamura, and T. Komurasaki.** 2003. A novel homocysteine-responsive gene, smap8, modulates mitogenesis in rat vascular smooth muscle cells. Eur. J. Biochem. 270:2521–2531.
20. **Okuda, T., and H. Kondoh.** 1999. Identification of new genes *Ndr2* and *Ndr3* which are related to *Ndr1/RTP/Drg1* but show distinct tissue specificity and response to N-myc. Biochem. Biophys. Res. Commun. 266:208–215.
21. **Piquemal, D., D. Joulia, P. Balaguer, A. Basset, J. Marti, and T. Commes.** 1999. Differential expression of the *RTP/Drg1/Ndr1* gene product in proliferating and growth arrested cells. Biochim. Biophys. Acta 1450:364–373.
22. **Qu, X., Y. Zhai, H. Wei, C. Zhang, G. Xing, Y. Yu, and F. He.** 2002. Characterization and expression of three novel differentiation-related genes belong to the human NDRG gene family. Mol. Cell. Biochem. 229:35–44.
23. **Salnikow, K., W. G. An, G. Melillo, M. V. Blagosklonny, and M. Costa.** 1999. *Nickel-induced* transformation shifts the balance between HIF-1 and p53 transcription factors. Carcinogenesis 20:1819–1823.
24. **Salnikow, K., T. Kluz, M. Costa, D. Piquemal, Z. N. Demidenko, K. Xie, and M. V. Blagosklonny.** 2002. The regulation of hypoxic genes by calcium involves c-Jun/AP-1, which cooperates with hypoxia-inducible factor 1 in response to hypoxia. Mol. Cell. Biol. 22:1734–1741.
25. **Shimono, A., T. Okuda, and H. Kondoh.** 1999. N-myc-dependent repression of *Ndr1*, a gene identified by direct subtraction of whole mouse embryo cDNAs between wild type and N-*myc* mutant. Mech. Dev. 83:39–52.
26. **Takagi, T., H. Moribe, H. Kondoh, and Y. Higashi.** 1998. DeltaEF1, a zinc finger and homeodomain transcription factor, is required for skeleton patterning in multiple lineages. Development 125:21–31.
27. **van Belzen, N., W. N. Dinjens, M. P. Diesveld, N. A. Groen, A. C. van der Made, Y. Nozawa, R. Vlietstra, J. Trapman, and F. T. Bosman.** 1997. A novel gene which is up-regulated during colon epithelial cell differentiation and down-regulated in colorectal neoplasms. Lab. Investig. 77:85–92.
28. **Wakisaka, Y., A. Furuta, K. Masuda, W. Morikawa, M. Kuwano, and T. Iwaki.** 2003. Cellular distribution of NDRG1 protein in the rat kidney and brain during normal postnatal development. J. Histochem. Cytochem. 51: 1515–1525.
29. **Xu, B., L. Lin, and N. S. Rote.** 1999. Identification of a stress-induced protein during human trophoblast differentiation by differential display analysis. Biol. Reprod. 61:681–686.
30. **Yagi, T., S. Nada, N. Watanabe, H. Tamemoto, N. Kohmura, Y. Ikawa, and S. Aizawa.** 1993. A novel negative selection for homologous recombinants using diphtheria toxin A fragment gene. Anal. Biochem. 214:77–86.
31. **Zhou, D., K. Salnikow, and M. Costa.** 1998. Cap43, a novel gene specifically induced by Ni^{2+} compounds. Cancer Res. 58:2182–2189.
32. **Zhou, R. H., K. Kokame, Y. Tsukamoto, C. Yutani, H. Kato, and T. Miyata.** 2001. Characterization of the human NDRG gene family: a newly identified member, NDRG4, is specifically expressed in brain and heart. Genomics 73:86–97.

Available online at www.sciencedirect.com
SCIENCE DIRECT®
Biochemical and Biophysical Research Communications 313 (2004) 647–653
BBRC
www.elsevier.com/locate/ybbrc

Pyridoxine 5′-phosphate oxidase is a candidate gene responsible for hypertension in Dahl-S rats☆,☆☆

Tomohiko Okuda, Toshiki Sumiya, Naoharu Iwai, and Toshiyuki Miyata*

National Cardiovascular Center Research Institute, 5-7-1 Fujishirodai, Suita, Osaka 565-8565, Japan

Received 8 October 2003

Abstract

To identify candidate genes responsible for hypertension in Dahl salt-sensitive rats (Dahl-S), an oligonucleotide microarray analysis was performed to find differentially expressed genes in kidneys of Dahl-S and Lewis rats. We obtained 101 F2 male rats from Dahl-S and Lewis rats and performed precise measurements of blood pressure (BP) and heart rate by telemetric monitoring at 14 weeks of age after 9 weeks of salt-loading. The correlation analysis between genotypes of differentially expressed genes and BP in F2 rats indicated that pyridoxine 5′-phosphate oxidase (*Pnpo*) and catecholamine-*O*-methyltransferease (*Comt*) showed a highly significant association with BP. However, in the case of *Comt*, the Dahl-S genotype correlated with low BP. Short/branched chain acyl-CoA dehydrogenase and *Sah* also showed a significant association with systolic blood pressure. The present study provided evidence that *Pnpo* is a candidate gene responsible for hypertension in Dahl-S rats.

Keywords: Hypertension; Dahl salt-sensitive rats; Blood pressure; Telemetry; Mammalian genetics; Pyridoxine 5′-phosphate oxidase

Hypertension is a major risk factor for cardiovascular morbidity and mortality. Blood pressure (BP) is known to be affected by genetic factors and is heritable. The identification of genes contributing to essential hypertension in humans is difficult because hypertension is a multifactorial disease resulting from environmental and genetic factors. To overcome this difficulty and facilitate genetic analyses, genetically hypertensive rat strains have been utilized [1]. Among them, the Dahl salt-sensitive rat (Dahl-S) and the spontaneously hypertensive rat (SHR) have been intensively investigated. Through analyses with these animals, many quantitative trait loci (QTLs) for BP were identified [2]. Usually, a QTL distributes in a large area on a chromosome and contains many genes, thus specifying that the genes responsible for hypertension are quite difficult. Furthermore, problems accompanied by errors of BP measurement should be considered. Conventionally, parameters such as BP or heart rate (HR) are collected by the tail-cuff method for QTL analysis. With this method, the rats are conscious and restrained, hence an error of measurement is inevitable. A precise BP measurement of the rats under freely moving condition using telemetry is desirable.

Recently, the identification of causative genes for phenotypes such as insulin-resistance of the spontaneously hypertensive rat has been successful [3]. This approach consisted of a combination of two independent methods, a microarray analysis for gene expression and mapping using a congenic strain. It can be speculated that some causative genes will be differentially expressed, thus candidates can be sought among the genes found to be differentially expressed [4,5]. We previously adopted an expression analysis using oligonucleotide microarrays to identify genes expressed differently between the SHR and normotensive Wistar–Kyoto rats [6,7].

The Dahl-S rat is a well-investigated model of salt-sensitive hypertension [2]. Using this model, many QTLs associated with BP have been identified [8,9].

☆ Supplementary data associated with this article can be found, in the online version, at doi:10.1016/j.bbrc.2003.11.149.

☆☆ *Abbreviations:* BP, blood pressure; Dahl-S, Dahl salt-sensitive rat; SHR, spontaneously hypertensive rat; QTL, quantitative trait locus; HR, heart rate; PNPO, pyridoxine 5′-phosphate oxidase; SBP, systolic blood pressure; DBP, diastolic blood pressure; COMT, catecholamine-*O*-methyltransferease; ACADSB, short/branched chain acyl-CoA dehydrogenase; SNP, single nucleotide polymorphism.

* Corresponding author. Fax: +81-6-6835-1176.
E-mail address: miyata@ri.ncvc.go.jp (T. Miyata).

0006-291X/$ - see front matter © 2003 Elsevier Inc. All rights reserved.
doi:10.1016/j.bbrc.2003.11.149

Detailed analyses using congenic strains have also been performed [9–15]. However, no definite genes responsible for hypertension have been reported to date. In the present study, to identify candidate genes responsible for hypertension, we combined an expression analysis of differentially expressed genes in the kidneys of Dahl-S and Lewis rats with a cosegregation analysis of F2 rats. The kidney is thought to be important not only as a target organ of hypertension but also as an organ that may cause hypertension [16]. Furthermore, to obtain precise data for 24-h BPs and HRs of rats, we adopted telemetric measurements. Using this strategy, pyridoxine 5′-phosphate oxidase (*Pnpo*) was identified as a candidate gene responsible for hypertension in Dahl-S rats. Three other genes were also implicated.

Materials and methods

Animals. Male Dahl–Iwai salt-sensitive rats (Sunplanet, Tokyo, Japan) were mated with female Lewis rats (Charles River Japan, Yokohama, Japan). The F1 offspring were intercrossed to produce 101 F2 male rats. These rats were bred under constant temperature (22 °C) and lighting (lights on at 7 a.m. and off at 7 p.m.) throughout the experiments. The rats were fed a normal rat chow (0.5% NaCl) (Clea Japan, Tokyo, Japan) and tap water ad libitum.

Measurement of blood pressure by telemetry. The F2 rats were fed an 8% NaCl-containing diet (Oriental Yeast, Tokyo, Japan) starting at 5 weeks of age. Indwelling radiotelemetric transmitters (TA11PA-C20, Data Sciences, St. Paul, MN) were implanted into the peritoneal cavities of 9-week-old rats and connected to the lower abdominal aortas. The transmitter signals were coded in a pulse position modulated serial bit stream, which is received and monitored by the receiver (RPC-1, Data Sciences) placed underneath the animal's cage. The data were collected for 10 s every 5 min continuously day and night and stored on a hard disk. At 14 weeks of age, the systolic blood pressure (SBP), diastolic blood pressure (DBP), and HR of F2 rats were measured continuously for 24 h, and the data were analyzed using Fluclet TM software (Dainippon Pharmaceutical, Osaka, Japan). The 12-h averages of SBP and DBP during day-time or night-time were determined. At 15 weeks of age, the rats were sacrificed and their body and heart weights were measured. The livers were also excised and the genomic DNA was extracted by the standard phenol/chloroform method. The present study was conducted in accordance with current guidelines for the care and use of experimental animals of the National Cardiovascular Center in Japan.

Expression analysis of kidney of Dahl-S and Lewis rats. Male Dahl-S and Lewis rats were fed an 8% NaCl diet starting at 10 weeks of age. At 15 weeks of age, rats were sacrificed and their kidneys were excised.

Table 1
Differentially expressed genes in kidneys of Dahl-S and Lewis rats

Gene description (*Symbol*)	Chromosome location	Expression change (S–L)	Fold change (S/L)	Diff. call	F2 analysis	Accession number
SA (*Sah*)	1q35	14,576	6.0	I	Done	S62516
Isovaleryl Coenzyme A dehydrogenase (*Ivd*)	3q35	8659	2.4	I	Done	AI102838
β-Galactoside-binding lectin (*Lgals1*)	7q34	7461	2.6	I		AI172064
Early growth response 1 (*Egr1*)	18q12.1	6449	2.1	I	Done	AF023087
P2x4 ATP receptor (*P2rx4*)	12q16	3369	2.8	I		U47031
Transgelin (*Tagln*)	8q24	2818	2.5	I		M83107
Membrane metallo endopeptidase (*Mme*)	2q31	2546	2.0	I	Done	AA894298
Vascular smooth muscle α-actin (*Acta2*)	1	2057	2.7	I		X06801
Renin (*Ren1*)	13q13	−2104	−7.9	D		S60054
2-Hydroxyphytanoyl-CoA lyase (*Hpcl2*)	16p16	−2286	−2.1	D		AA893239
UDP-glucuronosyltransferase (*Udpgt*)	14p21	−2359	−18.1	D	Done	M31109
Glutathione peroxidase 2 (*Gpx2*)	6q24	−3429	−4.3	D		AA800587
Cytosolic epoxide hydrolase (*Ephx2*)	15p12	−3509	−2.1	D		X60328
Insulin-like growth factor 1 (*Igf1*)	7q12-q13	−3621	−2.6	D		M15481
Pyridoxine 5 -phosphate oxidase (*Pnpo*)	10	−3745	−2.2	D	Done	U91561
Betaine homocysteine methyltransferase (*Bhmt*)	2q12	−3782	−2.3	D		AF038870
Cytochrome P-452 (*Cyp4a10*)	5q36	−4484	−2.0	D		X07259
Retinol dehydrogenase type 2 (*Rdh2*)	6q33	−4735	−4.2	D		U33500
Glutathione *S*-transferase 1 θ (*Gstt1*)	20p12	−5395	−2.5	D	Done	X67654
Short/branched chain acyl-CoA dehydrogenase (*Acadsb*)	1q34	−5493	−3.3	D	Done	U64451
Lipoprotein lipase (*Lpl*)	16p14	−6790	−3.0	D	Done	L03294
3-Hydroxy-3-methylglutaryl-CoA synthase (*Hmgcs2*)	2q34	−9581	−4.6	D	Done	M33648
Cytochrome P-450 IID5 (*Cyp2d5*)	7q34	−11,431	−2.1	D		J02869
Cytochrome P-450 M-1 (*Cyp2c*)	1q54	−11,713	−3.0	D		J02657
Retinol-binding protein (*Rbp4*)	1q54	−12,508	−5.1	D	Done	M10934
Cathechol-*O*-methyltransferase (*Comt*)	11q23	−13,576	−2.6	D	Done	M93257

Three independent experiments each for Dahl-S and Lewis rats were carried out and the average value is given. Genes with more than 2-fold and 2000 change in expression are listed.

Expression change (S–L), mean of the difference in intensity obtained by subtraction of the expression intensity in Lewis from that in Dahl-S ($n = 3$).

Fold change (S/L), mean of fold changes obtained by dividing the expression intensities in Dahl-S by those in Lewis ($n = 3$).

Diff. call, Difference call judged by the GeneChip Suite software; I, Increased; D, Decreased.

Total RNA was prepared with TRIzol reagent (Invitrogen, Carlsbad, CA) from excised whole kidney. Nine batches of total RNA from the Dahl-S and Lewis rats' kidneys were prepared, and three of each were pooled for poly(A)$^+$ RNA preparation. Procedures for the oligonucleotide microarray analysis were essentially identical as described [7]. For this analysis, the rat genome U34A arrays (Affymetrix, Santa Clara, CA; containing 8799 probe sets) were used. The resulting data were analyzed with GeneChip Suite Ver. 4.0 software (Affymetrix). A comparison analysis determined the differentially expressed genes as "increased (I)" or "decreased (D)". Three independent experiments for Dahl-S and Lewis were carried out, and those genes that met the following three criteria were considered to be candidate genes; the genes showed "I" or "D" two times or more in three comparisons, the average of difference change in three comparisons was greater than 2000, and there was a greater than 2-fold difference in expression of a gene.

Identification of specific genetic polymorphisms. Specific genetic polymorphisms of the candidate genes between Dahl-S and Lewis rats were identified by sequencing. For searching the polymorphisms, the genomic PCR was performed using a HotStar Taq Master Mix kit (QIAGEN, Hilden, Germany). The PCR products were used as templates for direct single-pass sequencing using a BigDye Terminator v3.0 Cycle Sequencing Ready Reaction kit (Applied Biosystems, Foster City, CA). The reaction products were purified with a DyeEX 96 kit (QIAGEN) and analyzed on an ABI PRISM 3700 DNA analyzer (Applied Biosystems). The obtained sequences were examined for the presence of a polymorphism using the Sequencher software (Gene Codes, Ann Arbor, MI) followed by visual inspection.

Northern blot analysis. The total RNA used for Northern blot analysis was the same as for the expression analysis. In addition, total RNA from Dahl-S rats fed a normal diet was also prepared for Northern blot analysis. Total RNA was electrophoresed in a 1% agarose gel containing 2% formaldehyde (10 μg/lane) and transferred onto a nylon membrane. To synthesize specific probes for each gene, partial cDNA fragments were synthesized by RT-PCR using total RNA derived from Lewis kidneys as templates. The PCR products were subcloned using a TOPO-TA cloning kit (Invitrogen). Fluorescein-labeled specific probes were generated by PCR as described previously [17], with the partial cDNA fragment as a template. The sense and antisense primers were 5′-CCTAAGTTGCTTGTCTGGGC-3′ and 5′-AGGCCTCGACGGAAGACAAT-3′ for *Pnpo*, 5′-ATGCCGTTGGCTGCAGTCTC-3′ and 5′-GCTGCTCCCTCTCACATACG-3′ for catecholamine-*O*-methyltransferease (*Comt*), 5′-AGGTTCTGGCTGGATTTGATAG-3′ and 5′-CCCACTGACAGTCTTTGGCAGC-3′ for *Sah*, and 5′-AAACCAGGATGGCGGTGTCT-3′ and 5′-TAGTCAAAACATCCTTGGGC-3′ for short/branched chain acyl-CoA dehydrogenase (*Acadsb*). Hybridization and detection procedures using a DNA Thunder Chemiluminescence Reagent Plus (PerkinElmer Life Sciences, Boston, MA) were performed according to the manufacturer's instructions. Detection was performed using a LAS-1000plus image analyzer (Fuji Film, Tokyo, Japan).

Statistical analysis. Cosegregation analysis for genotype–phenotype correlation was performed by one-way ANOVA using StatView software (SAS Institute, Berkeley, CA). Differences with a probability of $p < 0.05$ were considered to be significant.

Table 2
Blood pressure by genotype for differentially expressed genes of F2 rats

Gene	Blood pressure by genotype (mean ± SE)			*P*		
	S/S	S/L	L/L	Additive	Dominant	Recessive
Pnpo						
n	24	58	19			
SBP (light), mmHg	133.80 ± 11.12	132.19 ± 11.72	123.97 ± 7.98	0.0085**	0.0024**	0.1745
DBP (light), mmHg	91.19 ± 8.43	89.71 ± 8.69	83.79 ± 6.72	0.0104*	0.0033**	0.1437
SBP (dark), mmHg	142.98 ± 10.37	140.26 ± 11.26	131.45 ± 8.55	0.0016**	0.0006**	0.0615
DBP (dark), mmHg	98.47 ± 8.29	96.52 ± 8.28	89.94 ± 6.60	0.0019**	0.0007**	0.0694
Comt						
n	28	54	19			
SBP (light), mmHg	132.28 ± 10.55	127.66 ± 11.23	138.76 ± 9.02	0.0007**	0.0008**	0.4960
DBP (light), mmHg	89.76 ± 8.77	86.99 ± 8.80	93.31 ± 5.99	0.0176*	0.0136*	0.5569
SBP (dark), mmHg	140.11 ± 9.94	136.04 ± 11.58	147.19 ± 7.60	0.0006**	0.0005*	0.6379
DBP (dark), mmHg	116.96 ± 9.25	113.61 ± 10.31	121.62 ± 6.53	0.0344*	0.0223*	0.6316
Sah						
n	22	46	33			
SBP (light), mmHg	137.33 ± 11.28	129.83 ± 11.41	128.49 ± 10.23	0.0108*	0.1208	0.0030**
DBP (light), mmHg	92.51 ± 8.88	88.54 ± 8.50	87.12 ± 8.11	0.0670	0.1385	0.0271*
SBP (dark), mmHg	144.48 ± 10.17	138.00 ± 11.48	137.51 ± 10.74	0.0445*	0.2793	0.0126*
DBP (dark), mmHg	120.27 ± 9.11	115.08 ± 10.00	114.57 ± 9.50	0.1944	0.4165	0.0708
Acadsb						
n	22	45	34			
SBP (light), mmHg	137.16 ± 11.33	129.01 ± 10.93	129.73 ± 11.02	0.0151*	0.4168	0.0039**
DBP (light), mmHg	92.35 ± 8.79	88.05 ± 7.98	87.94 ± 8.98	0.1107	0.4033	0.0355*
SBP (dark), mmHg	139.37 ± 11.45	136.74 ± 10.79	139.37 ± 10.46	0.0362*	0.9390	0.0185*
DBP (dark), mmHg	98.22 ± 8.01	94.65 ± 7.99	95.59 ± 9.17	0.2653	0.8989	0.1197

The values for blood pressure are expressed as the 12-h mean in day time and night time.

SBP, systolic blood pressure; DBP, diastolic blood pressure; S, allele for Dahl-S rats; L, allele for Lewis rats; *P* value was obtained from one-way analysis of variance.

* $P < 0.05$.

** $P < 0.01$.

Results

Differentially expressed genes in Dahl-S and Lewis rats

We performed a gene expression analysis of kidneys from Dahl-S and Lewis rats with oligonucleotide microarrrays. As a result, 26 differentially expressed genes were identified as candidates for further analysis (Table 1). For the cosegregation analysis, exons or introns of these candidate genes of Dahl-S and Lewis rats were sequenced. Genetic polymorphisms to distinguish the genotypes between the two strains were identified in 12 genes (Supplementary Table 1). Most of the polymorphisms we identified were single nucleotide polymorphisms (SNPs). Unfortunately, we could not identify the polymorphisms in the remaining 14 genes.

F2 cosegregation analysis

We performed a cosegregation analysis of the genetic polymorphisms with various phenotypic parameters including BPs, HR, and body weight and heart weight in an F2 population (Tables 2 and 3). The PCR primers used for genotyping of the 12 candidate genes are listed in Supplementary Table 1. *Pnpo* exhibited a significant association with SBP and DBP of both day time and night time in the additive and dominant models (Table 2). In *Pnpo*, F2 rats with the Dahl-S (S) genotype showed a significantly increased BP compared to those with the Lewis (L) genotype. The BP of night time, when the rats are active, was more strongly correlated with the genotype than in the day time. *Comt* showed a significant association with SBP and DBP in the additive and dominant models. However, the heterozygotes showed a lower BP than either type of homozygote. Furthermore, F2 rats with the Lewis (L) genotype showed a significantly higher BP than those with the Dahl-S (S) genotype. Both *Sah* and *Acadsb* showed a significant association with SBP in the additive and recessive models. In both genes, F2 rats with the Dahl-S (S) genotype showed a significantly increased BP than those with the Lewis (L) genotype. None of them showed an association with HR (Table 3). *Comt* showed a significant association with body weight and heart weight in the additive and dominant models. *Sah* and *Acadsb* showed a significant association with heart weight in all statistical models.

Table 3
Heart rate, body weight, and heart weight by genotype for differentially expressed genes of F2 rats

Gene	Physiological parameters by genotype (mean ± SE)			*P*		
	S/S	S/L	L/L	Additive	Dominant	Recessive
Pnpo						
n	24	58	19			
HR (light), beats/min	295.80 ± 10.42	290.74 ± 11.21	292.94 ± 12.90	0.1855	0.8052	0.0916
HR (dark), beats/min	351.67 ± 10.91	350.73 ± 14.85	347.93 ± 12.44	0.6462	0.3730	0.6049
Body weight, g	371.75 ± 18.20	364.72 ± 23.66	370.00 ± 21.32	0.3623	0.5693	0.2694
Heart weight, g	1.255 ± 0.11	1.238 ± 0.12	1.212 ± 0.11	0.5026	0.3071	0.4046
Comt						
n	28	54	19			
HR (light), beats/min	291.08 ± 9.12	292.63 ± 13.19	293.46 ± 9.29	0.7598	0.6420	0.4892
HR (dark), beats/min	348.32 ± 13.34	352.00 ± 14.25	349.09 ± 11.54	0.4529	0.6329	0.3322
Body weight, g	365.07 ± 21.61	363.48 ± 22.53	381.90 ± 15.34	0.0051**	0.0012**	0.5166
Heart weight, g	1.25 ± 0.12	1.21 ± 0.11	1.31 ± 0.12	0.0039**	0.0031**	0.5946
Sah						
n	22	46	33			
HR (light), beats/min	292.75 ± 12.94	293.31 ± 11.76	290.77 ± 10.04	0.6169	0.3334	0.8570
HR (dark), beats/min	347.68 ± 14.43	350.22 ± 14.11	352.57 ± 12.00	0.4212	0.2710	0.2819
Body weight, g	362.73 ± 17.45	371.31 ± 23.86	364.91 ± 21.85	0.2352	0.4348	0.2650
Heart weight, g	1.28 ± 0.11	1.24 ± 0.12	1.20 ± 0.11	0.0268*	0.0189*	0.0385*
Acadsb						
n	22	45	34			
HR (light), beats/min	291.39 ± 12.83	293.30 ± 11.84	291.73 ± 10.13	0.7575	0.6980	0.6562
HR (dark), beats/min	345.41 ± 14.71	350.62 ± 13.93	353.43 ± 11.43	0.0938	0.1131	0.0483*
Body weight, g	368.45 ± 20.60	369.69 ± 22.34	363.76 ± 22.76	0.4728	0.2270	0.7988
Heart weight, g	1.30 ± 0.13	1.24 ± 0.12	1.19 ± 0.09	0.0038**	0.0062**	0.0056**

The values for heart rate (HR) are expressed as the 12-h mean in day time and night time.
S, allele for Dahl-S rats; L, allele for Lewis rats; *P* value was obtained from one-way analysis of variance.
* $P < 0.05$.
** $P < 0.01$.

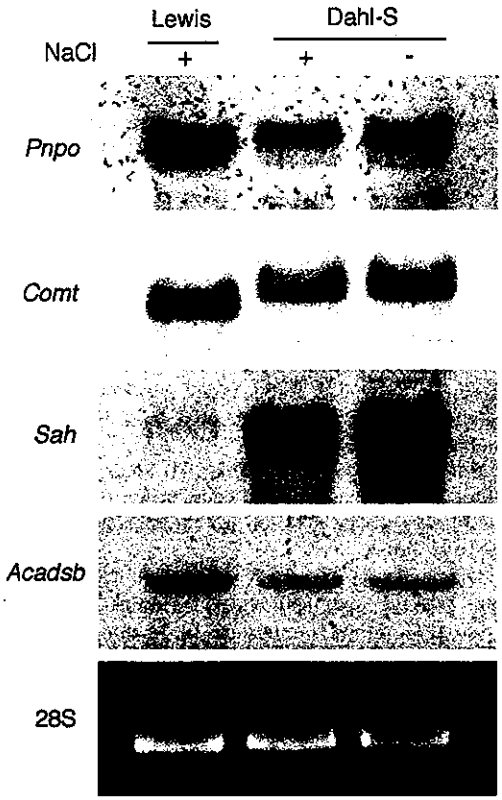

Fig. 1. Northern blot analysis of *Sah*, *Pnpo*, *Comt*, and *Acadsb*. Total RNA (10 μg per lane) obtained from kidneys of Lewis rats fed a high sodium diet, Dahl-S rats fed a high sodium diet, and Dahl-S rats fed a normal diet was used. The mRNAs of *Pnpo* and *Comt* genes from Dahl-S rats were apparently longer.

Northern blot analysis of candidate genes responsible for hypertension

Northern blot analysis for *Pnpo*, *Comt*, *Sah*, and *Acadsb* was performed using total RNA obtained from kidneys of Lewis rats fed a high sodium diet, Dahl-S rats fed a high sodium diet, and Dahl-S rats fed a normal diet (Fig. 1). The differential expression of these genes observed in the microarray analysis was confirmed by Northern blot analysis. It was also revealed that the transcript sizes of *Pnpo* and *Comt* were different between Dahl-S and Lewis rats. These results indicate that some insertion/deletion polymorphisms are present in these strains. To identify the insertion/deletion, we sequenced the PCR products from the genomic DNA of two rat strains. In the 3′-UTR region of *Pnpo*, we identified a 117-bp insertion in Dahl-S rats (data not shown). In *Comt*, an insertion (about 200 bp) was also detected in the 3′-UTR region of Dahl-S rats (data not shown).

Discussion

In the present study, we examined changes in gene expression in the kidneys of Dahl-S and Lewis rats with a microarray analysis and identified 26 differentially expressed genes. We generated 101 F2 rats whose BPs were monitored by telemetry. A cosegregation analysis of 12 differentially expressed genes using the F2 rats revealed that four genes, *Pnpo*, *Comt*, *Sah*, and *Acadsb*, showed a significant correlation with BP.

Among these four genes, *Pnpo* showed a highly significant association with BP (Table 2). PNPO (EC 1.4.3.5) catalyzes the oxidation of either the C4′ alcohol group or amino group of the two substrates pyridoxine 5′-phosphate and pyridoxamine 5′-phosphate to an aldehyde, forming pyridoxal 5′-phosphate (PLP; vitamin B_6) [18]. PNPO is a rate-limiting enzyme in the biosynthesis of PLP, which is a critical vitamin for normal cellular function [19]. The chromosomal location of the rat *Pnpo* gene was not clear in the current version of the database (rat build 2) at the National Center for Biotechnology Information (NCBI; http://www.ncbi.nlm.nih.gov/). The human *PNPO* gene is located between glial fibrillary acidic protein (*GFAP*) and nerve growth factor receptor (*NGFR*) on chromosome 17q21.32. The genes neighboring human *PNPO* are located on rat chromosome 10 [20]. Thus, the rat *Pnpo* gene is likely to be on chromosome 10. Rat chromosome 10 has been reported to contain two QTLs for BP [12,21,22] and one is syntenic to a human QTL for BP on chromosome 17 [23,24]. The *Pnpo*-neighboring genes, such as *Ngfr*, were located in a QTL for BP [23,24]. Therefore, the rat *Pnpo* gene was considered to be located within the QTL for BP. Considering these results, *Pnpo* is a candidate gene responsible for hypertension.

COMT (EC 2.1.1.6) is a ubiquitous enzyme that catalyzes the transfer of a methyl group from *S*-adenosylmethionine to catecholamines, including the neurotransmitters dopamine, epinephrine, and norepinephrine. This O-methylation is one of the major degradative pathways for the catecholamine transmitters. COMT plays an important role in the pathophysiology of disorders such as estrogen-induced cancers, Parkinson's disease, depression, and hypertension [25]. *Comt*-deficient mice exhibited changes in catecholamine levels and behavior [26]. Homozygous *Comt*-deficient female mice exhibited an impairment of emotional reactivity and heterozygous *Comt*-deficient mice displayed increased aggressive behavior [26]. Thus, *Comt* gene dosage may affect BP through individual behavior. We found a significant reduction of *Comt* expression in the kidney of Dahl-S rats and an insertion in the 3′-UTR region of *Comt* of Dahl-S rats that may affect the mRNA stability, leading to a reduction of COMT activity. The *Comt* gene would affect BP through catecholamine metabolism.

Sah was originally identified as a differentially expressed gene in the kidneys of SHR and Wistar–Kyoto rats [4]. *Sah* is located on rat chromosome 1q35 and has been reported to be related to hypertension [27]. It is

interesting that *Sah* was abundantly expressed in kidney of not only SHR but also Dahl-S rats, even in the salt-unloaded condition (Fig. 1). This implies a relationship between *Sah*-dosage and susceptibility to hypertension. *Acadsb* also demonstrated a significant correlation with BPs. ACADSB is a mitochondrial enzyme involved in the metabolism of fatty acids or branched-chain amino acids. A mutation in the *ACADSB* gene causes methylbutyrylglycinuria [28]. *Acadsb* is located on rat chromosome 1q34, close to the *Sah* locus. Both the *Sah* and *Acadsb* loci are located in a QTL for BP [29]. Thus, in addition to *Sah*, *Acadsb* would be a candidate gene responsible for hypertension.

There are several limitations to the present study. We could not identify the polymorphisms in the remaining 14 genes that are differentially expressed in kidneys. Those genes were not analyzed in the present study. The number of F2 rats in the present study ($n = 101$) may have been too small for precise detection of the genes responsible for hypertension.

In conclusion, we successfully identified *Pnpo* on rat chromosome 10 as a candidate gene responsible for hypertension in Dahl-S rats. In addition, we provided evidence that *Comt* on chromosome 11 and *Sah* and *Asadsb* both on chromosome 1 are likely involved in hypertension in Dahl-S rats. The significance of these genes in hypertension in humans will be addressed in future analyses.

Acknowledgments

We are grateful to Yoko Miyamoto for her technical assistance. This study was supported by the Program for Promotion of Fundamental Studies in Health Science of the Organization for Pharmaceutical Safety and Research of Japan.

References

[1] G.T. Cicila, Strategy for uncovering complex determinants of hypertension using animal models, Curr. Hypertens. Rep. 2 (2000) 217–226.
[2] J.P. Rapp, Genetic analysis of inherited hypertension in the rat, Physiol. Rev. 80 (2000) 135–172.
[3] T.J. Aitman, A.M. Glazier, C.A. Wallace, L.D. Cooper, P.J. Norsworthy, F.N. Wahid, K.M. Al-Majali, P.M. Trembling, C.J. Mann, C.C. Shoulders, D. Graf, E. St Lezin, T.W. Kurtz, V. Kren, M. Pravenec, A. Ibrahimi, N.A. Abumrad, L.W. Stanton, J. Scott, Identification of *Cd36* (*Fat*) as an insulin-resistance gene causing defective fatty acid and glucose metabolism in hypertensive rats, Nat. Genet. 21 (1999) 76–83.
[4] N. Iwai, T. Inagami, Isolation of preferentially expressed genes in the kidneys of hypertensive rats, Hypertension 17 (1991) 161–169.
[5] G.T. Cicila, S.J. Lee, Identifying candidate genes for blood pressure quantitative trait loci using differential gene expression and a panel of congenic strains, Hypertens. Res. 21 (1998) 289–296.
[6] T. Okuda, T. Sumiya, K. Mizutani, N. Tago, T. Miyata, T. Tanabe, H. Kato, T. Katsuya, J. Higaki, T. Ogihara, Y. Tsujita, N. Iwai, Analyses of differential gene expression in genetic hypertensive rats by microarray, Hypertens. Res. 25 (2002) 249–255.
[7] T. Okuda, T. Sumiya, N. Iwai, T. Miyata, Difference of gene expression profiles in spontaneous hypertensive rats and Wistar–Kyoto rats from two sources, Biochem. Biophys. Res. Commun. 296 (2002) 537–543.
[8] A.Y. Deng, In search of hypertension genes in Dahl salt-sensitive rats, J. Hypertens. 16 (1998) 1707–1717.
[9] M.R. Garrett, H. Dene, R. Walder, Q.Y. Zhang, G.T. Cicila, S. Assadnia, A.Y. Deng, J.P. Rapp, Genome scan and congenic strains for blood pressure QTL using Dahl salt-sensitive rats, Genome Res. 8 (1998) 711–723.
[10] G.T. Cicila, O.I. Dukhanina, T.W. Kurtz, R. Walder, M.R. Garrett, H. Dene, J.P. Rapp, Blood pressure and survival of a chromosome 7 congenic strain bred from Dahl rats, Mamm. Genome 8 (1997) 896–902.
[11] J.P. Rapp, M.R. Garrett, H. Dene, H. Meng, B. Hoebee, G.M. Lathrop, Linkage analysis and construction of a congenic strain for a blood pressure QTL on rat chromosome 9, Genomics 51 (1998) 191–196.
[12] O.I. Dukhanina, H. Dene, A.Y. Deng, C.R. Choi, B. Hoebee, J.P. Rapp, Linkage map and congenic strains to localize blood pressure QTL on rat chromosome 10, Mamm. Genome 8 (1997) 229–235.
[13] Q.Y. Zhang, H. Dene, A.Y. Deng, M.R. Garrett, H.J. Jacob, J.P. Rapp, Interval mapping and congenic strains for a blood pressure QTL on rat chromosome 13, Mamm. Genome 8 (1997) 636–641.
[14] G.T. Cicila, C. Choi, H. Dene, S.J. Lee, J.P. Rapp, Two blood pressure/cardiac mass quantitative trait loci on chromosome 3 in Dahl rats, Mamm. Genome 10 (1999) 112–116.
[15] A.Y. Deng, H. Dene, J.P. Rapp, Congenic strains for the blood pressure quantitative trait locus on rat chromosome 2, Hypertension 30 (1997) 199–202.
[16] K. Abe, S. Ito, The kidney and hypertension, Hypertens. Res. 20 (1997) 75–84.
[17] K. Kokame, H. Kato, T. Miyata, Homocysteine-respondent genes in vascular endothelial cells identified by differential display analysis, J. Biol. Chem. 271 (1996) 29659–29665.
[18] J.D. Choi, M. Bowers-Komro, M.D. Davis, D.E. Edmondson, D.B. McCormick, Kinetic properties of pyridoxamine (pyridoxine)-5′-phosphate oxidase from rabbit liver, J. Biol. Chem. 258 (1983) 840–845.
[19] E.O. Ngo, G.R. LePage, J.W. Thanassi, N. Meisler, L.M. Nutter, Absence of pyridoxine-5′-phosphate oxidase (PNPO) activity in neoplastic cells: isolation, characterization, and expression of PNPO cDNA, Biochemistry 37 (1998) 7741–7748.
[20] H. Zimdahl, T. Kreitler, C. Gosele, D. Ganten, N. Hubner, Conserved synteny in rat and mouse for a blood pressure QTL on human chromosome 17, Hypertension 39 (2002) 1050–1052.
[21] M.R. Garrett, X. Zhang, O.I. Dukhanina, A.Y. Deng, J.P. Rapp, Two linked blood pressure quantitative trait loci on chromosome 10 defined by Dahl rat congenic strains, Hypertension 38 (2001) 779–785.
[22] Z. Sivo, B. Malo, J. Dutil, A.Y. Deng, Accelerated congenics for mapping two blood pressure quantitative trait loci on chromosome 10 of Dahl rats, J. Hypertens. 20 (2002) 45–53.
[23] J. Baima, M. Nicolaou, F. Schwartz, A.L. DeStefano, A. Manolis, I. Gavras, C. Laffer, F. Elijovich, L. Farrer, C.T. Baldwin, H. Gavras, Evidence for linkage between essential hypertension and a putative locus on human chromosome 17, Hypertension 34 (1999) 4–7.
[24] D. Levy, A.L. DeStefano, M.G. Larson, C.J. O'Donnell, R.P. Lifton, H. Gavras, L.A. Cupples, R.H. Myers, Evidence for a gene influencing blood pressure on chromosome 17. Genome scan linkage results for longitudinal blood pressure phenotypes in subjects from the framingham heart study, Hypertension 36 (2000) 477–483.

[25] T. Xie, S.L. Ho, D. Ramsden, Characterization and implications of estrogenic down-regulation of human catechol-*O*-methyltransferase gene transcription, Mol. Pharmacol. 56 (1999) 31–38.

[26] J.A. Gogos, M. Morgan, V. Luine, M. Santha, S. Ogawa, D. Pfaff, M. Karayiorgou, Catechol-*O*-methyltransferase-deficient mice exhibit sexually dimorphic changes in catecholamine levels and behavior, Proc. Natl. Acad. Sci. USA 95 (1998) 9991–9996.

[27] S. Frantz, J.R. Clemitson, M.T. Bihoreau, D. Gauguier, N.J. Samani, Genetic dissection of region around the Sa gene on rat chromosome 1: evidence for multiple loci affecting blood pressure, Hypertension 38 (2001) 216–221.

[28] B.S. Andresen, E. Christensen, T.J. Corydon, P. Bross, B. Pilgaard, R.J. Wanders, J.P. Ruiter, H. Simonsen, V. Winter, I. Knudsen, L.D. Schroeder, N. Gregersen, F. Skovby, Isolated 2-methylbutyrylglycinuria caused by short/branched-chain acyl-CoA dehydrogenase deficiency: identification of a new enzyme defect, resolution of its molecular basis, and evidence for distinct acyl-CoA dehydrogenases in isoleucine and valine metabolism, Am. J. Hum. Genet. 67 (2000) 1095–1103.

[29] L. Gu, H. Dene, A.Y. Deng, B. Hoebee, M.T. Bihoreau, M. James, J.P. Rapp, Genetic mapping of two blood pressure quantitative trait loci on rat chromosome 1, J. Clin. Invest. 97 (1996) 777–788.

ELSEVIER

Atherosclerosis 173 (2004) 301–307

ATHEROSCLEROSIS

www.elsevier.com/locate/atherosclerosis

Identification of 21 single nucleotide polymorphisms in human hepatocyte growth factor gene and association with blood pressure and carotid atherosclerosis in the Japanese population

Shin Takiuchi [a,*], Toshifumi Mannami [b], Toshiyuki Miyata [c], Kei Kamide [a], Chihiro Tanaka [c], Yoshihiro Kokubo [b], Yuko Koyama [b], Nozomu Inamoto [b], Tomohiro Katsuya [e], Naoharu Iwai [c], Yuhei Kawano [a], Toshio Ogihara [e], Hitonobu Tomoike [d]

[a] *Division of Hypertension and Nephrology, Department of Medicine, National Cardiovascular Center, 5-7-1, Fujishirodai, Suita, Osaka 565-8565, Japan*

[b] *Division of Preventive Cardiology, National Cardiovascular Center, Suita, Osaka, Japan*

[c] *Research Institute, National Cardiovascular Center, Suita, Osaka, Japan*

[d] *Department of Medicine, National Cardiovascular Center, Suita, Osaka, Japan*

[e] *Department of Geriatric Medicine, Osaka University Graduate School of Medicine, Suita, Osaka, Japan*

Received 21 July 2003; accepted 15 December 2003

Abstract

It has been suggested that circulating concentrations of hepatocyte growth factor (HGF) are increased in individuals with vascular endothelial damage, such as in hypertensive patients and subjects with atherosclerosis. Because the influence of genetic variation of *HGF* has not been examined, we identified single nucleotide polymorphisms (SNPs) in the *HGF* gene, and investigated the association between these SNPs and blood pressure or carotid atherosclerosis in the Japanese general population. We identified 21 SNPs in the *HGF* gene by direct sequencing in a test population of 32 Japanese subjects. Among them, considering allele frequency and linkage disequilibrium, three SNPs, *C-1652T* in the promoter, *T43839A* in intron 8, and *T44222C* in intron 9, were genotyped in 2412 members of the Japanese general population randomly selected from the residents in Suita city. None of the three SNPs were significantly associated with blood pressure. After adjusting for age, smoking habits, consumption of alcohol, and the presence of diabetes mellitus and dyslipidemia, female subjects with the T allele of *T43839A* had more severe carotid atherosclerosis compared to individuals with the A allele. This study provides the first evidence that *HGF* may be a candidate susceptibility loci that affects the progression of atherosclerosis in Japanese subjects.

Keywords: Hepatocyte growth factor; Hypertension; Atherosclerosis; Genetics; Polymorphism

1. Introduction

Endothelial cell dysfunction has been suggested as the initiating process in the development and progression of cardiovascular disease, and it is considered to be closely related to the pathophysiology of human essential hypertension. There has been accumulating evidences that hepatocyte growth factor (HGF), mesenchyme-derived pleiotropic factor, plays an important role in endothelial cell dysfunction. Since HGF was originally identified in the plasma of rats after partial hepatectomy [1], a number of investigations have suggested that HGF is a multifunctional factor implicated in tissue regeneration and angiogenesis in not only liver but also other tissues [2,3]. A local HGF system (HGF and its receptor, c-met) is expressed in vascular cells [4], and elevated serum HGF levels have been suggested to play a cardiovascular protective role in hypertensive subjects, especially those with concomitant arteriosclerosis [5–9].

Although an association between HGF and the severity of hypertension was established, few reports have investigated the association between *HGF* gene polymorphisms and blood pressure or atherosclerosis. The *HGF* gene is composed of 18 exons encompassing 70 kb on chromosome 7q11.2-q21 [10]. In the present study, we screened for sin-

* Corresponding author. Tel.: +81-6-6833-5012; fax: +81-6-6872-7486.
E-mail address: takiuchi@hsp.ncvc.go.jp (S. Takiuchi).

0021-9150/$ – see front matter © 2004 Elsevier Ireland Ltd. All rights reserved.
doi:10.1016/j.atherosclerosis.2003.12.020

gle nucleotide polymorphisms (SNPs) in the *HGF* gene and evaluated the significance of SNPs in high blood pressure and carotid atherosclerosis determined by an ultrasonography using a large cohort, the Suita Study, which was representative of the general Japanese population.

2. Methods

2.1. Subjects

The protocol of the Suita Study, described elsewhere [11–14], was approved by the Ethics Committee of the National Cardiovascular Center. The sample consisted of 14,200 Japanese men and women ages 30–79 years stratified by gender and 10-year age groups, selected randomly from the municipal population registry. They were all invited by letter to attend regular cycles (every 2 years) of follow-up examinations. DNA from leukocytes was collected from participants who visited the Division of Preventive Medicine, National Cardiovascular Center between May 1996 and February 1998. Subjects who gave their written informed consent for genetic analyses of the genes were included in the present study. All clinical data and genotyping results were anonymous, and all data was handled in such a way that it was/will not be possible to identify an individual.

The characteristics of the subjects analyzed in the present study are summarized in Table 1. Blood pressure was measured in the subjects after at least 10 min of rest in a sitting position. Systolic blood pressure (SBP) and diastolic blood pressure (DBP) values are the mean of two physician-obtained measurements (recorded >3 min apart). Hypertension was defined as SBP ≥140 mm Hg or DBP ≥90 mm Hg or the current use of antihypertensive medications; diabetes mellitus was defined as fasting blood glucose ≥126 mg/dl, or the current use of insulin or oral anti-diabetic agents; and dyslipidemia was defined total cholesterol ≥220 mg/dl or the current use of antidyslipidemia medication at the time of the first examination.

Table 1
Clinical Features of Study Participants

Variables	Men n = 1158	Women n = 1254
Age, y	61.0 ± 12.2*	58.9 ± 11.7
Body mass index, kg/m2	23.1 ± 2.8*	22.3 ± 3.1
Systolic blood pressure (SBP), mmHg	129.2 ± 10.1	128.5 ± 21.1
Diastolic blood pressure (DBP), mmHg	81.0 ± 10.9*	78.8 ± 10.6
Total cholesterol (TC), mg/dL	204.6 ± 31.9	215.9 ± 32.9*
HDL cholesterol, mg/dL	54.1 ± 14.5	64.2 ± 15.6*
Current alcohol consumer (%)	38.0†	8.6
Current smoker (%)	71.5†	29.1
Hypertension (%)	39.6†	35.5
Diabetes mellitus (%)	9.1†	3.7
Dyslipidemia (%)	35.2	51.3†

Values are means ± SDs or percentages.
Hypertension indicates SBP ≥ 140 mmHg and/or DBP ≥90 mmHg or antihypertensive medication; Dyslipidemia, TC ≥ 220 mg/dL or antidyslipidemia medication; diabetes mellitus, fasting plasma glucose ≥ 126 mg/dL or antidiabetic medication.
* $P < 0.05$ between men and women by Student's t test.
† $P < 0.05$ between men and women by χ^2 test.

2.2. Evaluation of carotid atherosclerosis

Carotid ultrasonography was performed for the evaluation of atherosclerosis. Measurement methods were previously described [11,12]. Briefly, ultrasonography of both carotid arteries was performed with a high-resolution Duplex scanner (TOSHIBA SSA-250A; probe, SMA-736S mechanical sector scanner, Toshiba, Tokyo, Japan) for the B-scan. The subjects were examined in the supine position with their head slightly turned from the sonographer. All measurements were performed by two trained sonographers, who were unaware of the subjects' clinical data. The carotid arteries were carefully examined with regard to wall changes from different longitudinal (anterior oblique, lateral, and posterior oblique) and transverse views, and measurements of thickness were performed from transverse image. Intima-medial thickness (IMT) was measured at a point 10 mm proximal from the beginning of the dilatation of the carotid bulb, and Maximum-IMT (Max-IMT) was defined as the maximum thickness of intima-media including plaques from the region branching off from the brachiocephalic artery (right) or aorta (left) to the bifurcation of the common carotid artery. Plaque Score was calculated by summing the maximum thickness of all the plaques in the bilateral carotid artery in the scanning area [11,12].

2.3. Direct sequencing for the detection of polymorphisms in the HGF genes

We obtained peripheral blood samples from 32 Japanese volunteers for direct sequencing of the *HGF* gene after obtaining written informed consent. Genomic DNA was extracted with an NA-3000 nucleic acid isolation system (KURABO, Osaka, Japan). Methods of direct sequencing are described previously [15]. Briefly, all exons, a portion of introns and a region up-stream of exon 1, which included the promoter region of *HGF*, were amplified by polymerase chain reaction (PCR). The PCR products were then treated with shrimp alkaline phosphates and exonuclease I (PCR Product Pre-Sequencing Kit, USB Corporation, Cleveland, OH), and used as templates for direct single-pass sequencing using a BigDye Terminator v3.0 Cycle Sequencing Ready Reaction kit (Applied Biosystems, Foster City, CA). The reaction products were purified with a DyeEX 96 kit (QIAGEN) and analyzed on an ABI PRISM 3700 DNA analyzer (Applied Biosystems). The obtained sequences